MODELING AND CONTROL OF THE INTELLIGENT BUILDING AGENTS LABORATORY

by

Laith Abdulmajeid

A thesis submitted in partial fulfillment of

the requirements for the degree of

Master of Science

(Mechanical Engineering)

at the

UNIVERSITY OF WISCONSIN–MADISON

2023

ACKNOWLEDGMENTS

He who does not thank people (for their favors) has not thanked Allah

— Prophet Muhammad, peace and blessings be upon him

Writing this section while being flooded with emotions, the day has finally come when I can proudly say that: I did it!

Throughout this journey, I was extremely fortunate to have many supportive people by my side, embedding and reinforcing my love for engineering, science, and knowledge. Not only do they support me intellectually, but they are also kind, beautiful individuals who never fail to show care and thoughtfulness. Even though words would not do them justice, I will take this opportunity to acknowledge them to my best abilities.

To everyone I call family: Thank you for always being here for me even when some of you could not be physically here. I always feel grateful to have such amazing people in my life, who not only push me to grow and be a better version of myself, but also teach me to acknowledge my accomplishments and be kind to myself. You always lend me the strength and desire to keep pursuing growth, and I will be forever in your debt. Hopefully, I will pay it back by contributing to improving the quality of life of those around us.

To my advisors: Thank you Greg for getting me hooked on thermal sciences from the first day in undergrad. From Intro to ME to graduate-level heat transfer, you have always succeeded effortlessly in stimulating my desire to learn more. I probably would not be writing this thesis if you hadn't believed in me and invited me to join the Solar Energy Lab as an undergraduate researcher. It has always been an honor and pleasure to have you as a mentor. Thank you Mike for bringing me into the fascinating world of optimization. Working with you closely, you have always made me feel encouraged to ask any question and to not only pursue the "how", but the "why" as well. Thank you for

always being patient, benevolent, and caring from day one. I'm truly grateful that I can call you a mentor and a friend. Thank you Doug for giving me a peek into the world of HVAC. Admittedly, I don't think I admired enough the intricacy of such crucial systems before starting this project. For systems that highly impact our quality of life, you have always amazed me with your vast knowledge and expertise, which you did not hesitate in the slightest to share and communicate flawlessly. Thank you for your patience and mentorship.

Special thanks to Amanda Pertzborn for answering all my questions about the IBAL and for showing me around that impressive facility. This research would not be possible without your prompt support for inquiries and data collection. I would also like to acknowledge David Bradly for his help with TRNSYS. Thank you for showing me the ropes and always answering my debugging questions.

And to everyone I met at the Solar Energy Lab: Thank you for being such amazing friends and peers. Especially Matt Mullin, thank you for being a close friend and having a positive impact on my life. You never failed to amaze me and always added a special delight to our endless thought-provoking discussions.

Finally, this research was only made possible with the grant funded by NIST (NIST Award # 70NANB21H108).

CONTENTS

Contents iii

List of Tables v

List of Figures vi

Nomenclature xi

Abstract xiii

1 Introduction 1

1.1 Motivation 1

1.2 The Intelligent Building Agents Laboratory 2

1.3 TRNSYS Simulation Software 4

1.4 Project Scope 5

2 Literature Review 6

2.1 Building Energy Systems Modeling 6

2.2 Air-side System Model 8

3 Hydronic System Modeling 10

3.1 Introduction 10

3.2 Chillers 11

3.3 Thermal Energy Storage 18

3.4 Flow Hydraulics Calculation 22

4 Hydronic System Control 30

4.1 Supervisory Controllers 30

4.2 Model Predictive Controller 37

4.3 Local Controllers 42

5 Complete IBAL Model 46

5.1 Model Integration 46

5.2 Operation Modes 47

5.3 User Interface 48

6 Conclusions 67

7 Future Work 68

References 70

LIST OF TABLES

3.1 Capacity, Capacity ratio, COP, and COP ratio for TRNSYS Type 666 given a rated Capacity and COP of 27.3 kW and 3.18, respectively — Chiller 1 model. 17

3.2 Capacity, Capacity ratio, COP, and COP ratio for TRNSYS Type 666 given a rated Capacity and COP of 36 kW and 4.13, respectively — Chiller 2 model. . 18

3.3 Fraction of full-load power and PLR for TRNSYS Type 666 — Chiller 1 and Chiller 2 model. 18

3.4 Inputs, outputs, and parameters for TRNSYS Type 9008—the thermal energy storage model. 22

4.1 Inputs, outputs, and parameters for TRNSYS Type 9001—the hydronic system control model. 32

4.2 Inputs, outputs, and parameters for TRNSYS Type 9002—the primary loop/chiller temperature setpoint control model. 35

4.3 Inputs, outputs, and parameters for TRNSYS Type 9003—the secondary loop differential pressure setpoint control model. 37

5.1 The primary mode signals for the IBAL based on the mode algorithm presented 48

LIST OF FIGURES

1.1 A simplified schematic of the IBAL system. Components inside the red solid border simulate the outdoor air and the occupancy impact on the HVAC system. Components inside the blue dashed border simulate the building equipment to be controlled. 3

3.1 Schematic of the IBAL hydronic system 11

3.2 Chiller 2 capacity as a function of chilled water temperature at two different cooling water temperatures from experimental data 13

3.3 Chiller COP as a function of chilled water temperature at two different cooling water temperatures from experimental data 14

3.4 Chiller capacity ratio normalized by the rated condition as a function of chilled water temperature at two different cooling water temperatures from experimental data 15

3.5 Chiller COP ratio normalized by the rated condition as a function of chilled water temperature at two different cooling water temperatures from experimental data 16

3.6 Chiller 2 fraction of full-load power as a function of part-load ratio at $T_{cw} =$ 23.89C at different $T_{chw,sp}$, from experimental data 17

3.7 Schematic of the hydronic loop illustrating the flow rates that the flow hydraulic calculations Type solves. 23

3.8 Schematic of the hydronic loop illustrating the flow rates that the flow hydraulic calculations Type solves. 26

3.9 Normalized pump head as a function of normalized flow rate for pump 3 . . 27

3.10 Maximum head and flow at a given pump speed for pump 3 27

3.11 Normalized pump power as a function of normalized flow rate for pump 3. . 28

3.12 Maximum power consumption at a given pump speed for pump 3 29

4.1 A pictorial representation of the supervisory controllers responsible for regulating the hydronic system's response to "building" load. The solid line represents the setpoint temperature while the dotted line represents the differential pressure setpoint 31
4.2 A visualization of a model predictive controller responding as a function of time [1] 38
4.3 The local PI control loop for the TES valve position which regulates the primary loop outlet temperature 43
4.4 The local PI control loop for the bridge valve position which regulates the secondary loop inlet temperature 44
4.5 The local PI control loop for the cooling coil valve position which regulates the AHU supply air temperature 45

5.1 On the left axis, the outdoor air temperature $T_{air,outdoor}$ and the respective zone temperatures T_{Z1} and T_{Z2} are plotted. The zones are maintained at a setpoint temperature of 19C. On the right axis, the zones' sensible loads ($qSnsOcc_{Z1}$ and $qSnsOcc_{Z2}$) are plotted indicating the presence of occupants in the zones 51
5.2 On the right axis, the temperatures of the tank's inlet T_{in} and outlet T_{out} are shown, as well as the leaving temperature after mixing $T_{out,mixed}$ with the TES bypass. On the left axis, the state of charge of the tank ice_{inve} is plotted and can be seen decreasing as the TES is discharged 51
5.3 The heat transfer rates are plotted for different components in the IBAL. Since the TES is used to fully meet the demand, it can be seen that the TES heat transfer rate Q_{TES} is equivalent in absolute value to that of the air handling unit $Q_{AHU,liq}$. 52

5.4 On the left axis, the preheating signals ($HeaterSig_{Z1}$ and $HeaterSig_{Z2}$) are plotted as it shows the varying intensity of the VAV heaters. On the right axis, the VAV damper positions ($DamperPos_{Z1}$ and $DamperPos_{Z2}$) and the zone temperatures are both plotted on the same axis. 53

5.5 On the left axis, the temperatures of the air leaving $T_{cc,air,out}$ and the chilled water entering $T_{CC,pg,in}$ are shown. On the right axis, the chilled water flow rate $CoolantFlow$ is shown to demonstrate how it is modulated to maintain the supply air setpoint temperature. 54

5.6 On the left axis, the outdoor air temperature $T_{air,outdoor}$ and the respective zone temperatures T_{Z1} and T_{Z2} are plotted. The zones are maintained at a setpoint temperature of 19C. On the right axis, the zones' sensible loads ($qSnsOcc_{Z1}$ and $qSnsOcc_{Z2}$) are plotted indicating the presence of occupants in the zones 54

5.7 On the left axis, Chiller 2 power consumption $CH2_{Power}$ is plotted. On the right axis, the simulated chilled water temperature $T_{CH2,out}$, along with the set points for both the chilled water T_{CHWST} and primary loop temperatures $T_{PL,out}$ 55

5.8 The heat transfer rates are plotted for different components in the IBAL. Since chiller 2 is used to fully meet the demand, it can be seen that the respective heat transfer rate Q_{CH2} is equivalent in absolute value to that of the air handling unit $Q_{AHU,liq}$. 56

5.9 On the left axis, the preheating signals ($HeaterSig_{Z1}$ and $HeaterSig_{Z2}$) are plotted as it shows the varying intensity of the VAV heaters. On the right axis, the VAV damper positions ($DamperPos_{Z1}$ and $DamperPos_{Z2}$) and the zone temperatures are both plotted on the same axis. 57

5.10 On the left axis, the temperatures of the air leaving $T_{cc,air,out}$ and the chilled water entering $T_{CC,pg,in}$ are shown. On the right axis, the chilled water flow rate $CoolantFlow$ is shown to demonstrate how it is modulated to maintain the supply air setpoint temperature. 57

5.11 On the left axis, the outdoor air temperature $T_{air,outdoor}$ and the respective zone temperatures T_{Z1} and T_{Z2} are plotted. The zones are maintained at a setpoint temperature of 19C. On the right axis, the zones' sensible loads ($qSnsOcc_{Z1}$ and $qSnsOcc_{Z2}$) are plotted indicating the presence of occupants in the zones 58

5.12 On the left axis, the temperature of the entering T_{in} and leaving T_{out} chilled water is plotted. Since the TES is being charged, the TES valve is fully open and all the flow goes through the TES; this is why the final mixed leaving temperature $T_{out,mixed}$ is omitted since there is no mixing. On the right axis, the TES state of charge ice_{inve} is plotted to demonstrate the charging process. 59

5.13 On the right axis, the power of chiller 2 $CH2_{Power}$ is plotted to demonstrate the charging process. On the right axis, the chilled water temperature $T_{CH2,out}$, and the set points for both the chilled water T_{CHWST} and primary loop outlet $T_{PL,out}$ temperatures 59

5.14 The inlet and outlet temperatures of the primary loop $T_{PL,in}$ and $T_{PL,in}$, respectively, as well as the inlet and outlet temperatures of the secondary loops $T_{SL,in}$ and $T_{SL,in}$, respectively. 60

5.15 On the left axis, the temperature of the air leaving $T_{cc,air,out}$ and the chilled water entering $T_{CC,pg,in}$ is shown. On the right axis, the chilled water flow rate $CoolantFlow$ is shown to demonstrate how it is modulated to maintain the supply air setpoint temperature while the chiller is charging the TES. . . . 61

5.16 Electricity price schedule based on a Time-of-Use structure. 62

5.17 Occupant thermal load from the zones represents the "building" load in the IBAL that the hydronic system responds to. 62
5.18 The MPC-generated primary mode schedule of the IBAL over an optimization period of 72 hours. Mode 1 uses TES to meet demand, mode 3 uses the chiller to meet demand, and mode 5 charges the TES with ice. 63
5.19 The state of the TES from the TRNSYS simulation using the MPC mode schedule. On the left axis, the TES inlet temperature T_{in}, and mixed outlet temperature $T_{out,mixed}$ are shown. On the right axis, the TES state of charge is plotted. 64
5.20 The predicted state of charge of the TES from the MPC solution. 64
5.21 The VAV boxes respond to maintain the zone temperature during the MPC-generated schedule TRNSYS simulation. On the left axis, the preheating signals ($HeaterSig_{Z1}$ and $HeaterSig_{Z2}$) are plotted as it shows the varying intensity of the VAV heaters. On the right axis, the VAV damper positions ($DamperPos_{Z1}$ and $DamperPos_{Z2}$) and the zone temperatures are both plotted on the same axis. 65
5.22 The heat transfer rates are plotted for different components in the IBAL during a simulation that uses an MPC-generated mode schedule. 66

DISCARD THIS PAGE

NOMENCLATURE

Abbreviations

IBAL	Intelligent Building Agents Laboratory
TES	Thermal Energy Storage
MPC	Model Predictive Controller
AHU	Air Handling Unit
CC	Cooling Coil
VAV	Variable Air Volume
HVAC	Heating, Ventilation, and Air Conditioning
NIST	National Institute of Standards and Technology

Variables [units]

c	Specific heat [kJ/kg-K]
Δ	Temperature difference [°C]
$\dot{m}$	Mass flow rate [kg/s]
COP	Coefficient of Performance [-]
T	Temperature [°C]

Subscripts

avg	Average
c	Cold Fluid
h	Hot Fluid
i	Index
chw	Chilled Water
cw	Cooling Water

nom	Nominal
SL	Secondary Loop
PL	Primary Loop
sp	Setpoint

ABSTRACT

This master's thesis presents the development and integration of the National Institute of Standards and Technology's (NIST) Intelligent Building Agents Laboratory (IBAL) HVAC system within the TRNSYS software environment. The project involved the development of TRNSYS components to model the hydronic side of the HVAC system while integrating with air-side models developed previously [2]. Furthermore, local controllers for individual system components were implemented to support the development of an optimization-based supervisory model predictive controller (MPC). The MPC is responsible for generating optimal schedules for operating an ice thermal storage tank in conjunction with chillers, which was implemented in a Python programming environment.

The objectives of this research were threefold: 1) Develop comprehensive and accurate models of the hydronic side of an HVAC system test facility. 2) Incorporate those models into an overall HVAC system model that also includes the previously developed air system models. 3) Optimize the energy performance of the total system. To achieve these goals, a detailed investigation of the hydronic side was conducted, leading to the development and tuning of TRNSYS components that accurately represented the system behavior. Simultaneously, the existing air-side models were integrated to establish a holistic and dynamic HVAC system simulation.

A core contribution of this thesis lies in developing an innovative optimization-based supervisory model predictive controller. This advanced controller leverages forecast data to predict system behavior, and automatically generate optimal schedules for operating the ice thermal storage tank. As a result, energy consumption cost was improved, and the overall HVAC system's performance was enhanced, particularly during peak load periods.

The significance of this research extends to the broader field of HVAC system design and operation. The integrated HVAC system test facility, along with the novel model predictive control strategies, offers a substantial potential for energy and cost savings and environmentally conscious practices. Moreover, the presented methodology and implementation framework serve as valuable references for future researchers in the energy-efficient HVAC system design field.

In conclusion, this master's thesis successfully models the IBAL HVAC system test facility using TRNSYS, as well as develops an optimization-based supervisory model predictive controller for optimal operation of an ice thermal storage tank. The results highlight the efficacy of the proposed approach in achieving improved energy performance and set a foundation for further advancements in sustainable HVAC systems.

1 INTRODUCTION

1.1 Motivation

In the U.S., commercial buildings consume 18% of the national energy demand; 40% of that demand accounts for Heating, Ventilation, and Air Conditioning (HVAC) systems [3]. The quest for net-zero energy buildings has intensified the focus on optimizing the energy efficiency of commercial buildings, particularly their HVAC systems. Despite significant progress in integrating building control systems through standard communication protocols like BACnet and BACnet/IP, there remains a critical lack of "intelligent" optimization capabilities at the system level that optimize overall building system performance [4].

Large buildings, characterized by complex HVAC systems comprising chiller units, air-handling units (AHU), and air distribution or terminal units, pose unique challenges in achieving optimal performance. Conventional HVAC control systems often encounter conflicts between the optimal operations of individual equipment components vs. the optimal operation of connected components comprising the system. For example, an AHU may perform optimally when receiving water at a specific temperature from the chiller, while the chiller itself may have better performance at a different water temperature.

To address these challenges, approaches based on an "intelligent agent" could be employed to enable distributed decision-making among the various HVAC equipment [4]. With intelligent agents, a control decision could be generated and communicated to another agent or executed, based on the agent's hierarchy. This thesis contributes to advancing intelligent HVAC controls by modeling the Intelligent Building Agents Laboratory (IBAL) HVAC test facility at the National Institute of Standards and Technology (NIST) and exploring optimal control methods for enhancing the energy performance of building HVAC systems.

1.2 The Intelligent Building Agents Laboratory

The IBAL provides the essential physical air conditioning systems infrastructure and computational foundation for the development and testing of advanced agent-based optimization methods, which are designed to enhance energy efficiency and comfort levels in expansive buildings. The IBAL is designed to emulate a large building's multi-zone HVAC system. This allows the IBAL to bridge the gap between different scientific domains (such as HVAC and artificial intelligence) and create a collaborative and interdisciplinary research environment. More importantly, the IBAL provides realistic HVAC systems to functionally evaluate and proof test control strategies for equipment and systems prior to deployment in actual systems in the field.

The term "large buildings" specifically denotes structures of ample size that encompass an HVAC system consisting of one or more chiller units, air-handling units (AHUs), and air distribution or terminal units. The optimization challenges presented by such HVAC systems are intricate and call for research to be conducted within a facility equipped with the capabilities afforded by the IBAL. Complete documentation on the details of the IBAL is presented in [5][6][7]. Figure 1.1 illustrates a simplified schematic of the IBAL system.

In Figure 1.1, the outdoor air handling unit's purpose is to emulate outdoor air under different conditions. This provides researchers with the capability to recreate different weather conditions repeatedly and consistently, offering flexibility for testing. The zone simulators are designed to emulate real building cooling loads that are imposed on HVAC systems. Each zone is designed to mimic a 65 m^2 in an office building. Combined, the four zones can emulate a sensible load of 20 kW and a latent load of 4.3 kW, summing up to a total load of 24 kW.

The AHU's role is to condition the emulated outdoor air accordingly; that is accomplished using a preheat coil and cooling coil downstream supplied with a chilled 30%

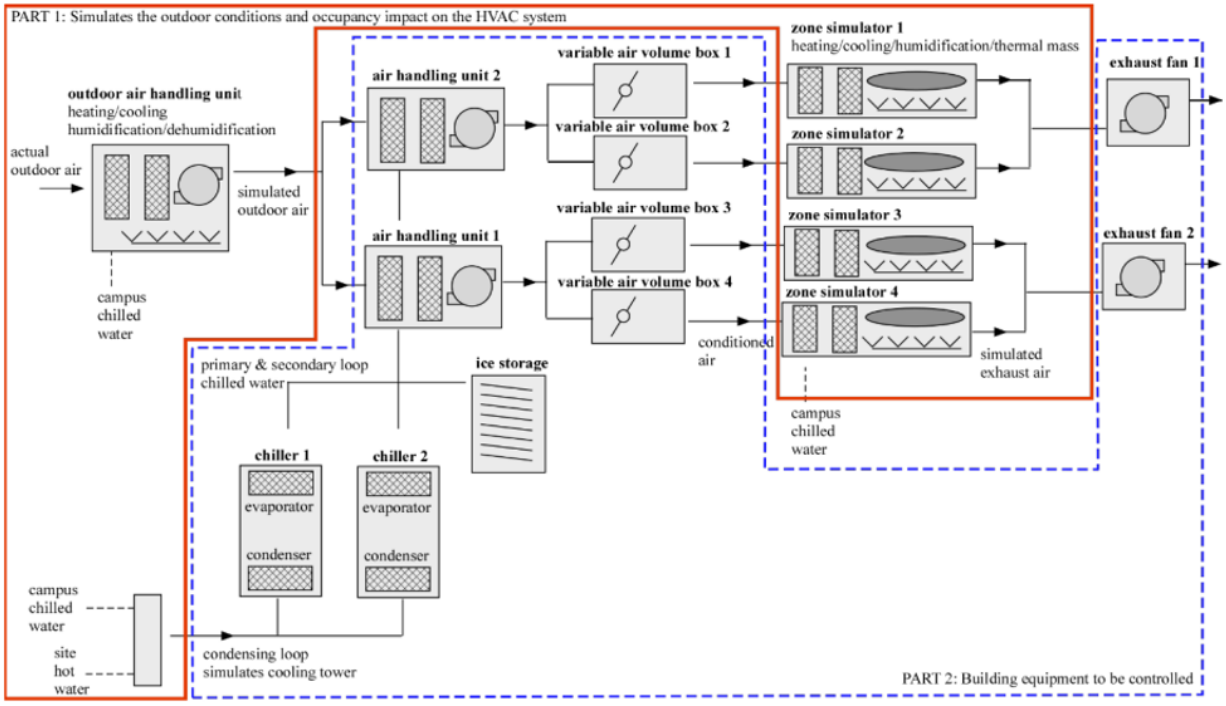

Figure 1.1: A simplified schematic of the IBAL system. Components inside the red solid border simulate the outdoor air and the occupancy impact on the HVAC system. Components inside the blue dashed border simulate the building equipment to be controlled.

propylene glycol coolant mixture circulated from the chillers and/or the ice storage. Once the air leaves the AHU, it is directed to the variable air volume (VAV) units that supply conditioned air to zones that simulate occupied spaces within a commercial office building. The VAV's role is to regulate the flow rates to satisfy the air-conditioning requirements of each zone via a damper and a reheat coil in each unit. Typically, the dampers have primary control over air regulation with a minimum setting based on occupancy, while the reheat coil is only activated during low load conditions where closing the damper beyond its minimum would be required to achieve the desired zone temperature.

The main chilling components in the system are two chillers and an ice-style thermal energy storage. Chiller 1 and Chiller 2 are rated at 26.4 kW and 36 kW of nominal capacity, respectively, while the thermal energy storage is rated at 274 kWh of ice storage. These components provide a chilled glycol-water mixture for the cooling coils that absorb the heat rejected from the AHU air stream. In the case of the chillers, they reject heat to the

emulated cooling tower located in the condensing loop; the cooling tower provides a heat sink for the system to reject heat. Combining the aforementioned components together, the IBAL has the ability to replicate the HVAC systems of different building designs, with varying load requirements, and most weather conditions.

1.3 TRNSYS Simulation Software

TRNSYS (pronounced 'tran-sis') stands as a highly adaptable software environment with a graphical interface, utilized to simulate the behavior of transient systems; it is primarily geared toward evaluating the efficacy of thermal and electrical energy systems [8]. TRNSYS's modular structure provides it with high adaptability, making it suitable for in-depth analyses of systems reliant on temporal dynamics; this has earned TRNSYS the status of a foundational software tool for researchers and engineers on a global scale.

TRNSYS consists of two main components. The first component is an engine known as the "kernel," which reads and processes input files, systematically solves the system, assesses convergence, and generates visual representations of system variables. The kernel also offers a range of utilities that encompass tasks like determining thermophysical properties, matrix inversion, linear regression, and interpolation of external data files.

The second component of TRNSYS is an extensive library of various components, each designed to model the performance of a distinct part of the system. The standard library includes around 150 models, spanning from pumps to multi-zone buildings, wind turbines to electrolyzers, weather data processors to economic routines, and fundamental HVAC equipment to cutting-edge emerging technologies. These models are structured in a manner that permits users to modify existing components or even craft new ones, thereby extending the capabilities of the software environment.

1.4 Project Scope

The central focus of this project lies in developing a comprehensive and accurate model of the hydronic, chilling, and thermal energy storage components used within the IBAL test facility for incorporation into the TRNSYS simulation environment. Special attention is given to the hydronic side, requiring the creation of custom TRNSYS components to represent the complex interactions involved in heat transfer and energy exchange processes. Subsequently, the Integration of the hydronic model with the previously developed air-side model [2] allows for a holistic simulation of the entire IBAL HVAC system.

Additionally, various control schemes are added to mimic the real IBAL response. The Model Predictive Controller (MPC) serves as one of the primary outcomes of this project, utilizing forecast data to predict system behavior and generate optimal schedules for operating an ice-on-coil thermal energy storage in conjunction with a chiller. This optimization-based supervisory MPC can play a crucial role in reducing energy consumption and improving overall HVAC system performance, particularly during peak load periods.

The findings presented in this thesis contribute significantly to the advancement of intelligent HVAC control methodologies, offering practical solutions for enhancing energy efficiency and environmental sustainability in large building systems. The TRNSYS model provides NIST with a valuable tool to use in conjunction with the physical facility to further the development of intelligent agents and optimization-based control strategies. This research seeks to play a key role in the journey towards net-zero energy buildings and a more sustainable future for the built environment.

2.1 Building Energy Systems Modeling

HVAC systems consist of various components that work in unison to serve the building's requirements as needed. With large building systems, the interactions between all the different components lead to a high-complexity, non-linear behavior to be modeled. Nonetheless, in order to build a model that captures the performance of such complex systems, components like chillers, pumps, air handling units, and more require their physics to be appropriately modeled.

Capturing the physics of energy systems can often be put into three categories: White-box, grey-box, and black-box models. Each approach comes with its own advantages and disadvantages and can excel in different use cases. Choosing the appropriate approach becomes important given the scope and the purpose of the model, therefore, an evaluation of each approach with respect to the project at hand is instrumental.

White-box models (often referred to as physics-based) utilize first-principles physics and mathematical relations to represent a system. Oftentimes, this modeling approach requires appropriate domain knowledge in the relevant areas (e.g. heat transfer for HVAC) and a good understanding of the system's inner workings. Based on the assumptions of the models, steady-state or dynamic models can be built to provide the required level of model fidelity [9]. This approach is commonly used during the design stage to simulate, scrutinize, and analyze HVAC systems. Given that physics is involved, white-box models are considered highly accurate but can become more computationally expensive as the physical behavior becomes more complex.

Black-box models (often referred to as data-driven) primarily use prior knowledge of a system's behavior through historical data to model and predict the system's states.

This approach does not necessarily require a deep understanding of the physical systems, but rather an extensive amount of data to capture the system's predicted response. By using mathematical relations, black-box models map the system's inputs to its outputs and can provide output predictions in a less computationally expensive manner than white-box models. The computational advantage does come with the penalty of the model's performance being highly reliant on the training data; this leads to restricting the model's inputs to within the training inputs ranges [9].

Grey-box models can be best described as a hybrid of white-box and black-box models. This approach combines the understanding of the system's physics with historical performance knowledge to identify relevant physical parameters (e.g. capacitance of a thermal mass) [9]. In many cases, the actual system behavior can differ from its theoretical response due to factors such as environmental effects (e.g. equipment aging) or physics assumptions. By combining both domain knowledge and historical inference, grey-box models can be an excellent choice for modeling existing systems, specifically for control purposes that require a clearly defined mathematical representation of the system's states.

In TRNSYS, the modeling framework primarily consists of white-box and grey-box models. In the case of simulating the IBAL, this framework makes TRNSYS an advantageous choice for capturing the complex performance of the IBAL's various components. By using physics-constrained models, the IBAL's response can be confidently predicted within a wide range of operating conditions. Additionally, with access to measurement instrumentation in the IBAL, equipment data can be gathered as needed to fine-tune the model's physical parameters.

2.2 Air-side System Model

In the previous stage of this project, a former Solar Energy Lab researcher at the University of Wisconsin-Madison developed the model for the IBAL's air-side system [2]. That process involved developing transient models for the cooling coils and heating elements that were tuned to capture the performance of their physical counterparts. Additionally, a model for the airflow and static pressures in the air-side system was developed and calibrated to reflect the real behavior of the system. Finally, multiple controllers were designed to mimic the control of the Variable Air Volume (VAV) boxes, the Air Handling Unit (AHU) fan, and the chilled water flow rate through the water side of the cooling coils.

The cooling coils (CC) are located in the AHU; their main purpose is to cool the air and/or dehumidify the air. The cooling process is accomplished by passing the air over tubes chilled with cold glycol circulating through them, effectively working as a heat exchanger between the air and water systems. Meanwhile, the heating elements are located prior to the cooling coil in the AHU; their purpose is to avoid freezing the cooling coil if the outdoor temperature is too cold. Both the CC model and the heating element model are conductance-based and incorporate a thermal capacitance to capture transient effects. Test data was collected to properly match their performance under varying flow conditions.

The airflow and static pressures in the air system are influenced by the fan's speed and the dampers' positions. Hence, a model was developed to calculate the flow rate and static pressure across each component. The fan is characterized by its pressure rise which is a function of flow rate and fan speed. Meanwhile, the dampers are captured by their pressure drop which is a function of flow rate and damper position. Both models were tuned using test data collected from the IBAL, which creates a model that can solve for the system's states, given information about the fan's speed and dampers' positions.

An effort has also been made to establish control logic that mimics the IBAL's air system control. The controllers developed were primarily inspired by the IBAL's actual control schemes and were translated into the TRNSYS simulation environment. The incorporated controllers modulate the VAV's damper position and reheat signal, the AHU fan speed, and the coolant flow through the CC. These controllers are developed as proof demonstrating the feasibility of controller models in an IBAL simulation.

Since the air system only accounts for half of the IBAL components, the hydronic system model is meant to augment the completed air system model. Similar approaches are followed in terms of developing models for the hydronic components, however, it might be deemed sufficient to only retain a high level of details instead. For instance, based on testing data it might be unnecessary to model capacitance effects in the chillers. due to their small magnitude relative to the intended use of the completed model.

A similar approach could be followed to model the hydronic flow rate and pressure system. The pumps are characterized by their pressure rise, which is a function of pump speed and flow rate. Meanwhile, the valves are captured by their pressure drops, which is a function of valve position and flow rate. Performance curves can be established from testing data and a similar model can be developed.

An effort is also established to develop control logic on both the supervisory and local control levels. Supervisory control is associated with high-level decisions that can impact the system's mode of operation. On the other hand, local control is involved in regulating a process relative to a reference value and the current process state. The hydronic system contains various controllers on both levels, therefore, their IBAL implementation is investigated and attempted to be translated to the TRNSYS simulation model.

3 HYDRONIC SYSTEM MODELING

3.1 Introduction

The hydronic system (commonly referred to as the "water-side" system) is part of the HVAC system that is responsible for supplying the working heat transfer fluid at a certain temperature to meet the air-side "building" demand. Building demand (or load) is defined as the energy added to the air from the zones, which needs to be removed to maintain the zones at a specific thermal condition. The hydronic system interfaces with the air-side system via the cooling coils in the air-handling units, where it extracts heat from the air stream before it is supplied to the occupant zones.

The IBAL's hydronic system uses a so-called "primary-secondary" configuration, where the secondary loop extracts heat from the "building" load via the AHU, and passes the absorbed heat to the primary loop that contains the chiller plant equipment. The chiller then absorbs heat from the glycol prior to recirculating to the cooling coils and then rejecting the absorbed heat to the condensing loop. The purpose of the condensing loop is to emulate a building's cooling tower; this provides the primary loop with a regulated water supply that acts as a heat sink for heat rejection.

Figure 3.1 illustrates a schematic of the hydronic system as built in the IBAL facility. In addition to the AHUs in the secondary loop, a heat exchanger is added that can emulate a building load, which enables running experiments without operating the air system. At the heart of the primary loop are two chillers, a thermal energy storage, and a heat exchanger that serves as a waterside economizer.

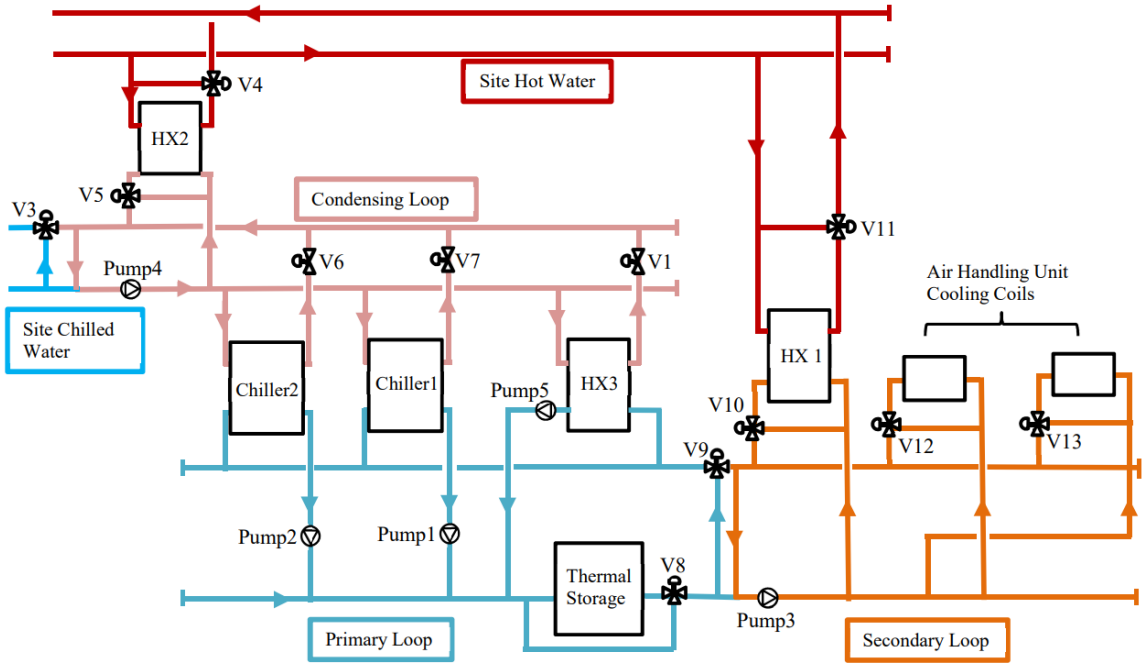

Figure 3.1: Schematic of the IBAL hydronic system

3.2 Chillers

A chiller is a refrigeration machine that is used to lower the temperature of a liquid. The chiller lowers the temperature of the working thermal fluid in the hydronic system, which consequently acts as a heat sink that removes energy from the air-side system. For large HVAC systems, separating the air from the chillers using a dedicated chilled water [1] system is more advantageous; some benefits include smaller piping requirements due to water's higher specific heat capacitance, as well as decoupling the chillers from the individual AHUs loads, which allows the chillers to serve multiple AHUs simultaneously.

The IBAL uses water-cooled vapor-compression cycle chillers located in the primary loop; thus, that type will be the focus of the modeling presented. In essence, the vapor-compression cycle is a closed, steady-state cycle wherein the working fluid undergoes a phase change as it moves around the various system components [10]. The cycle can

[1] water is commonly referenced in a broad sense, but specifically for the IBAL system, the circulating fluid comprises a mixture of glycol+water

be summarized in the following four stages: evaporation, compression, condensation, and expansion. Various models exist for capturing the performance of water-cooled vapor-compression chillers; one of the most commonly used in the energy modeling field is empirical-based models. These models utilize performance maps that are created using chiller operational data and capture the unique characteristics of each chiller.

In this case, the TRNSYS Type 666 is used which relies on catalog data to predict water-cooled chiller performance. To set up the model, the user needs to provide two text-based data files in the standard TRNSYS data file format. The first file is a set of values that map the chiller's capacity ratio and the coefficient of performance (COP) ratio to varying values of chilled-water setpoint temperature and entering cooling water temperature. Both ratios are obtained by normalizing with the chiller's rated condition. The second file is a set of values that map the chiller's fraction of full-load power (FFLP) to the part-load ratio (PLR) values.

The two IBAL chillers are characterized by conducting load ramping tests at varying operating conditions performed by NIST personnel. The collected variables of interest for the model are power consumption, COP, delivered cooling capacity, leaving chilled water temperature, and entering cooling water temperature. The test runs were performed at varying chilled water setpoint temperatures and cooling water temperatures for both chillers. Figure 3.2 and Figure 3.3 show the full-load cooling capacity and COP, respectively, at varying chilled-water setpoint temperatures and entering cooling water temperatures

The chiller full-load capacity is defined as the maximum cooling capacity it can provide at a given condition; these conditions are the leaving chilled water setpoint temperature and the entering cooling water temperature. Similarly, the full-load COP depends on those two variables as well. In order to provide the first data file to the TRNSYS model, both capacity and COP are normalized by their respective rated condition value of the specific chiller. Figure 3.4 illustrates the normalized capacity $\mathtt{Capacity}_{\mathtt{ratio}}$ and Figure

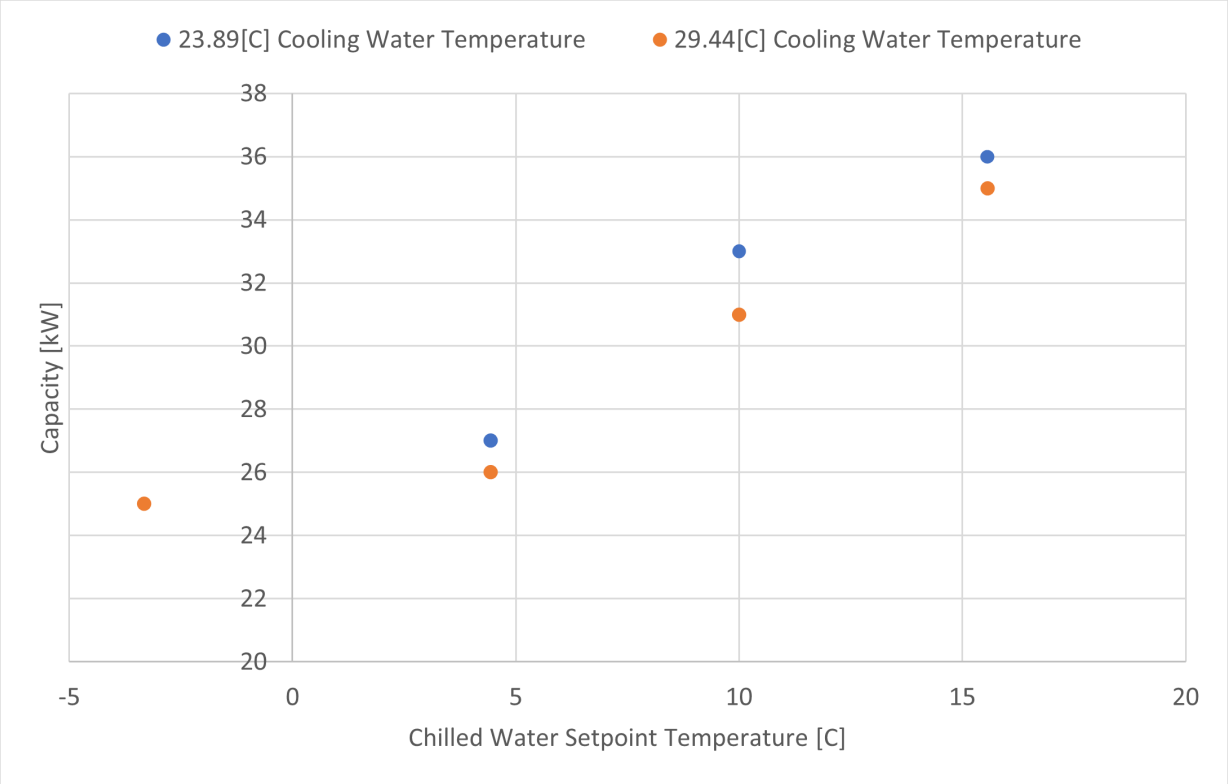

Figure 3.2: Chiller 2 capacity as a function of chilled water temperature at two different cooling water temperatures from experimental data

3.5 illustrates the normalized COP $\mathrm{COP}_{\mathrm{ratio}}$.

Additionally, the fraction of full-load power (FFLP) and the part-load ratio (PLR) can be mapped using testing data. The PLR is defined as the ratio of the delivered cooling capacity to the full-load capacity for the given conditions (leaving chilled water temperature and entering cooling water temperature), while the FFLP is defined as the ratio of power consumption at a given load relative to the full-load power consumption, both of which range from 0 to 1. Figure 3.6 shows an example of this relationship, as well as the independence of the FFLP from the operating conditions (i.e. T_{cw} or $\mathrm{T}_{\mathrm{chw,sp}}$) as all the curves collapse to a single curve.

The calculations done during each time step of the TRNSYS model start with Type 666 first calling the TRNSYS DynamicData routine with the current chilled water setpoint temperature and entering cooling water (sink) temperature. This returns the COP ratio

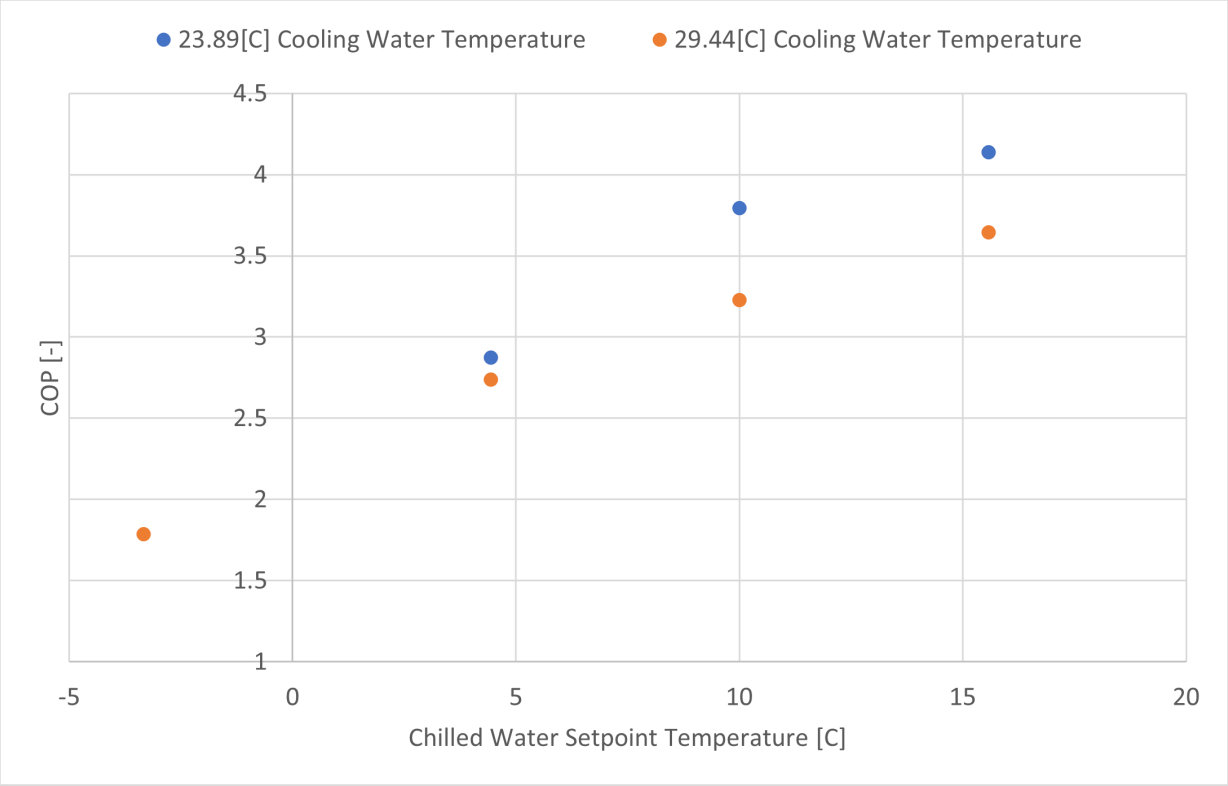

Figure 3.3: Chiller COP as a function of chilled water temperature at two different cooling water temperatures from experimental data

and capacity ratio for those conditions. The chiller's nominal COP and capacity at the current conditions are calculated using Equations 3.1 and 3.2, respectively.

$$\mathrm{COP}_{nom} = \mathrm{COP}_{rated}\ \mathrm{COP}_{ratio} \tag{3.1}$$

$$\mathrm{Capacity} = \mathrm{Capacity}_{rated}\ \mathrm{Capacity}_{ratio} \tag{3.2}$$

Capacity, as used here, represents the chiller's maximum cooling capability for the current conditions of leaving the chilled water temperature and entering the cooling water temperature. The chiller load is defined by an energy rate balance on the chilled water stream, which is calculated using Equation 3.3

$$\dot{Q}_{load} = \dot{m}_{chw}\ c_{chw}\ (T_{chw,in} - T_{chw,set}) \tag{3.3}$$

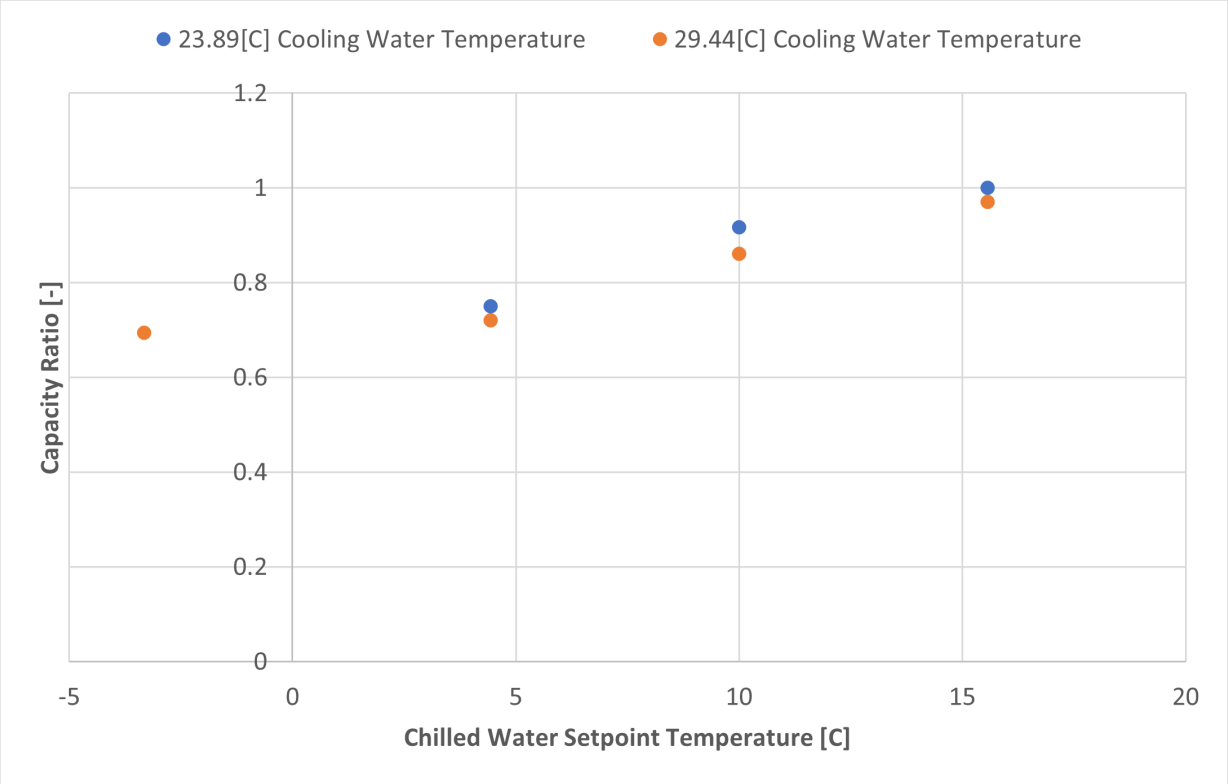

Figure 3.4: Chiller capacity ratio normalized by the rated condition as a function of chilled water temperature at two different cooling water temperatures from experimental data

Given the chiller load and its nominal capacity at the current conditions, the part load ratio is found using Equation 3.4

$$\text{PLR} = \frac{\dot{Q}_{load}}{\text{Capacity}} \tag{3.4}$$

If the chiller load is less than the chiller's current capacity, then the load met (the cooling that the chiller actually provides) is equivalent to the load applied to the chiller. However, if the load is greater than the current capacity, then the load met is capped by the current capacity. The resulting PLR, constrained between 0 and 1, is then used to perform a second call to the DynamicData routine for the second data file. This call returns the FFLP for the current conditions. The chiller's power consumption is then given by Equation 3.5

$$\text{P} = \frac{\text{Capacity}}{\text{COP}_{nom}} \text{FFLP} \tag{3.5}$$

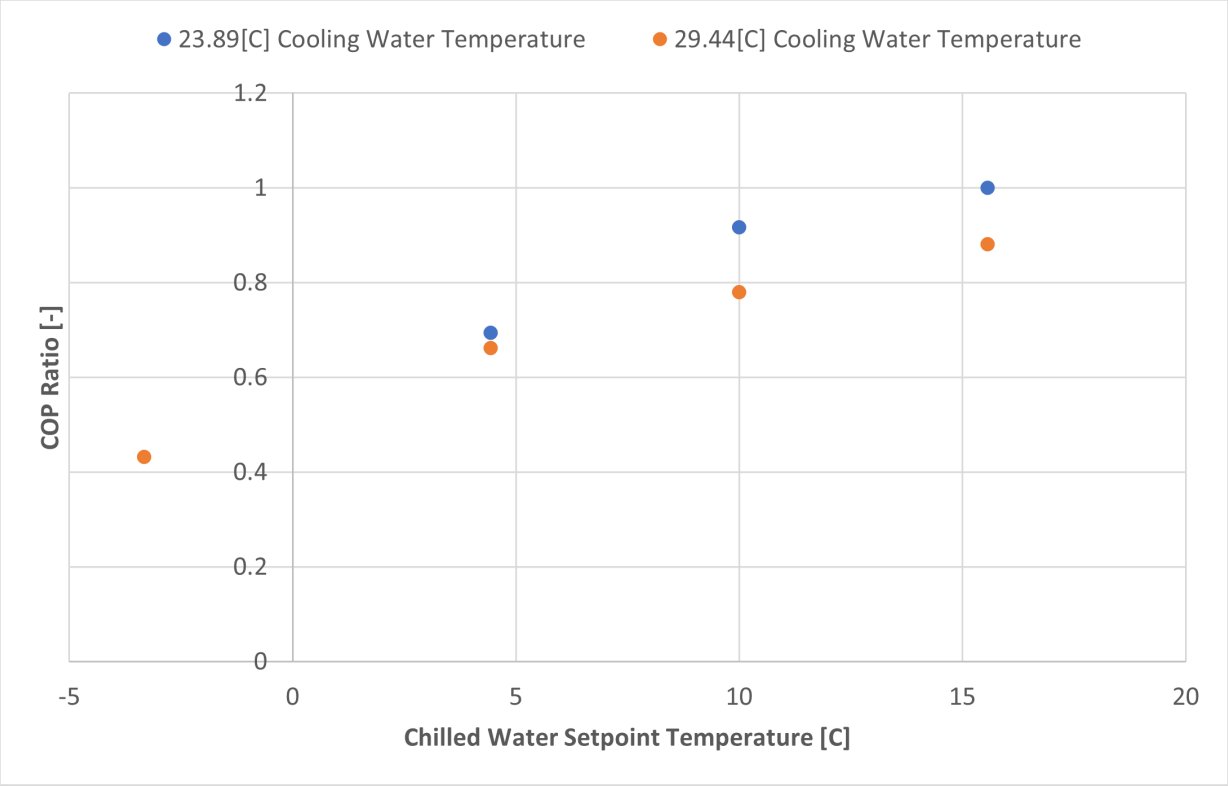

Figure 3.5: Chiller COP ratio normalized by the rated condition as a function of chilled water temperature at two different cooling water temperatures from experimental data

A new COP for the current conditions is then calculated using Equation 3.6

$$\mathrm{COP} = \frac{\dot{Q}_{met}}{P} \tag{3.6}$$

Subsequently, an energy rate balance is performed on the chiller to determine the heat rejected into the cooling fluid stream using Equation 3.7

$$\dot{Q}_{rejected} = \dot{Q}_{met} + P \tag{3.7}$$

Finally, the outlet temperature of the chilled fluid stream and the cooling water stream is then calculated by performing energy rate balances on each stream using Equations 3.8 and 3.9, respectively

$$T_{chw,out} = T_{chw,in} - \frac{\dot{Q}_{met}}{\dot{m}_{chw}\, c_{chw}} \tag{3.8}$$

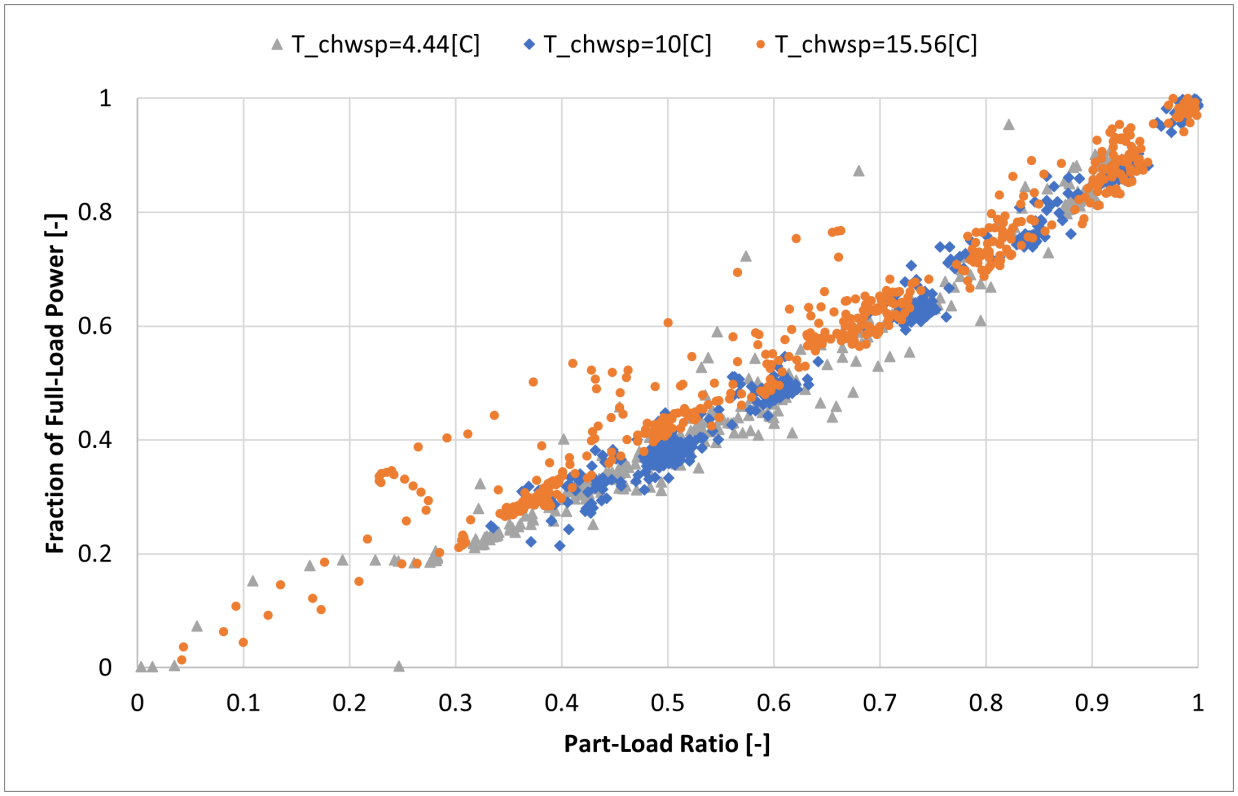

Figure 3.6: Chiller 2 fraction of full-load power as a function of part-load ratio at $T_{cw} = 23.89$C at different $T_{chw,sp}$, from experimental data

$$T_{cw,out} = T_{cw,in} + \frac{\dot{Q}_{rejected}}{\dot{m}_{cw}\, c_{cw}} \tag{3.9}$$

Table 3.1 and Table 3.2 document the values associated with the first data file for the TRNSYS Type 666 model for each chiller, respectively. Table 3.3 documents the FFLP values for varying PLR values for both chillers that are provided as the second TRNSYS data file.

Table 3.1: Capacity, Capacity ratio, COP, and COP ratio for TRNSYS Type 666 given a rated Capacity and COP of 27.3 kW and 3.18, respectively — Chiller 1 model.

$T_{chw,sp}$ [°C]	$T_{cw,in}$[°C]	**Capacity** [kW]	**Capacity ratio** [–]	**COP**[–]	**COP ratio**[–]
4.44	23.89	19	0.696	2.31	0.729
10	23.89	23	0.842	2.87	0.904
15.56	23.89	27.3	1	3.18	1
4.44	29.44	18	0.659	1.85	0.584
10	29.44	22.2	0.813	2.47	0.776
15.56	29.44	26.4	0.967	2.87	0.902
-3.33	29.44	14	0.513	1.75	0.55

Table 3.2: Capacity, Capacity ratio, COP, and COP ratio for TRNSYS Type 666 given a rated Capacity and COP of 36 kW and 4.13, respectively — Chiller 2 model.

$T_{chw,sp}$ [°C]	$T_{cw,in}$[°C]	**Capacity** [kW]	**Capacity ratio** [–]	**COP**[–]	**COP ratio**[–]
4.44	23.89	27	0.75	2.87	0.694
10	23.89	33	0.917	3.79	0.917
15.56	23.89	36	1	4.14	1
4.44	29.44	26	0.722	2.74	0.661
10	29.44	31	0.861	3.23	0.780
15.56	29.44	35	0.972	3.65	0.881
-3.33	29.44	25	0.694	1.79	0.432

Table 3.3: Fraction of full-load power and PLR for TRNSYS Type 666 — Chiller 1 and Chiller 2 model.

PLR[–]	FFLP[–]
0.2	0.20
0.3	0.20
0.4	0.35
0.5	0.40
0.6	0.50
0.7	0.60
0.8	0.75
0.9	0.85
1	1

3.3 Thermal Energy Storage

Thermal energy storage (TES) is a component that acts as a thermal battery for HVAC systems; it primarily shifts load from traditional HVAC equipment such as chillers. In the case of the IBAL, thermal energy storage in the form of an ice tank is used to accomplish that purpose. An ice tank is a component that is located in the primary loop of the hydronic system. Ice tanks work by using the plant's chillers to build ice (typically during off-peak hours) and storing that ice in the thermal storage tank, where it can be used at different times to produce chilled water for the secondary loop either with or without a chiller operation.

Ice tank modeling approaches vary in complexity depending on the level of fidelity desired for the application at hand. One approach for modeling ice tanks can be based on physics and heat transfer principles. This approach would capture the heat exchange process at a high-fidelity level and could consider material phase changes accordingly. Another approach could be based on empirical correlations that are tuned using experimental data. This approach could prove sufficient in certain modeling applications.

The IBAL contains an internal melt ice-on-coil style TES; these tanks are filled with water and are characterized by internal spiral heat-exchanging tubes that form ice around them when a low-temperature mixture of glycol/water mixture is passed through the tubes comprising the spiral heat exchanger. The tank can then be discharged by passing the warm glycol through the spiral heat exchanger, which releases its heat by melting the ice around the tubes. Since one of the primary objectives of this project is high-level decision-making and controls, modeling the intricate micro-level physics of the ice-on-coil was deemed unnecessary at this stage of the project. As a result, a simple physics-based NTU-effectiveness gray box heat exchanger model is developed that includes an empirical UA that is a function of the storage tank's state of charge (SOC).

This model simulates the charging and discharging of the TES and predicts the SOC and leaving water temperature at each time step. However, a limitation of this simplified model is that it assumes a constant temperature for the phase change material (i.e. water) throughout charge or discharge. As a result, the model only captures latent charging and does not account for any sensible portion of the TES tank during charging. Latent charging is when the water is at its freezing temperature and ice is forming. Practically speaking, these tanks only experience sensible charging during initial startup or after prolonged periods of shutdown when the water temperature is above its freezing temperature. As a consequence, the model cannot predict the storage behavior once it is fully discharged (SOC<0%).

In developing the UA correlation to SOC, the obtained experimental data was performed at a specific chilled water flow rate value. As the flow rate varies, the UA is also expected to vary, which could require a UA that is a function of both SOC and chilled water flow rate. As of now, it is assumed that those variations can be ignored, however, more testing data at varying flow rates would be needed to build a three-dimensional relationship for this model. Equation 3.10 and 3.11 represent the correlations used for the UA [W/(m^2·K)]during charging and discharging, respectively.

$$UA_{charge} = -10000 \cdot SOC + 15000 \tag{3.10}$$

$$UA_{discharge} = 10000 \cdot SOC + 2000 \tag{3.11}$$

The calculations done during each time step of the TRNSYS model can be described in the following steps:

1. Get the initial total energy [J] stored in the TES based on both the current SOC and the maximum energy capacity of the TES
2. Calculate the UA based on both the current SOC and the operation mode (charging/discharging)
3. Calculate the NTU using 3.12

$$NTU = \frac{UA}{\dot{m}_{fluid}\, c_{fluid}} \tag{3.12}$$

4. Given the assumption of constant phase change material temperature, the phase change material can be modeled as having infinite capacitance, and the respective

effectiveness-NTU correlation can be used using 3.13

$$\epsilon = 1 - \exp(-NTU) \tag{3.13}$$

5. The temperature of the fluid leaving can be solved for by rearranging the effectiveness definition in 3.14 in terms of the temperatures leaving using 3.15

$$\epsilon = \frac{T_{fluid,in} - T_{fluid,out}}{T_{fluid,in} - T_{ice}} \tag{3.14}$$

$$T_{fluid,out} = T_{fluid,in} - T_{fluid,in}\ \epsilon \tag{3.15}$$

6. Next, the rate of heat transfer can be solved with an energy balance on the fluid stream using 3.16

$$\dot{Q} = \dot{m}_{fluid}\ c_{fluid}\ (T_{fluid,out} - T_{fluid,in}) \tag{3.16}$$

7. Given the rate of heat transfer, the energy change per a given time step can be found using 3.17

$$\Delta E = \dot{Q}\ \Delta t \tag{3.17}$$

8. Finally, the SOC is updated using 3.18

$$SOC = SOC + \frac{\Delta E}{E_{max}} \tag{3.18}$$

Table 3.4 documents the inputs, outputs, and parameters associated with the TRNSYS model.

Table 3.4: Inputs, outputs, and parameters for TRNSYS Type 9008—the thermal energy storage model.

Symbol	Units	Default	Description
Parameters			
E_{max}	J	9.864×10^6	Maximum energy capacity
T_{ice}	°C	0.	Freezing temperature
c_{ice}	$J/(kg\cdot K)$	2108	Ice specific heat capacity
h_{fusion}	J/kg	334000	Ice latent heat of fusion
c_{fluid}	$J/(kg\cdot K)$	3890	water-glycol specific heat capacity
Inputs			
$\dot{m}_{fluid}$	kg/hr	4860	Glycol mass flow rate
$T_{fluid,in}$	°C	-3.66	Glycol inlet temperature
Outputs			
$T_{fluid,out}$	°C	-	Glycol outlet temperature
$\dot{Q}$	kJ/hr	-	Heat transfer rate
E_{total}	J	-	Total available energy
SOC	—	-	State of charge
ϵ	—	-	Heat exchange effectiveness

3.4 Flow Hydraulics Calculation

In order to fully capture the behavior of the hydronic system, a TRNSYS component is developed to solve for the flow rates and pressures at different locations throughout the primary and secondary loop. This model requires the pumps' speeds and the control valves' positions as inputs and returns the corresponding differential pressures and flow rates across the different elements of the hydronic system

The modeling approach used here is most often referred to as the "drain-pipe" theory, which draws analogies between electrical circuit components and their hydraulic equivalency. An example of that would be modeling pressure as electrical potential and flow rate as electrical current. This also entails that flow restrictions (e.g. valves) would be modeled as electrical resistors, which in this case dictate the amount of flow that goes through a given branch. Figure 3.7 shows a schematic of the hydronic system with the pumps, valves, and flow rates for which the model solves.

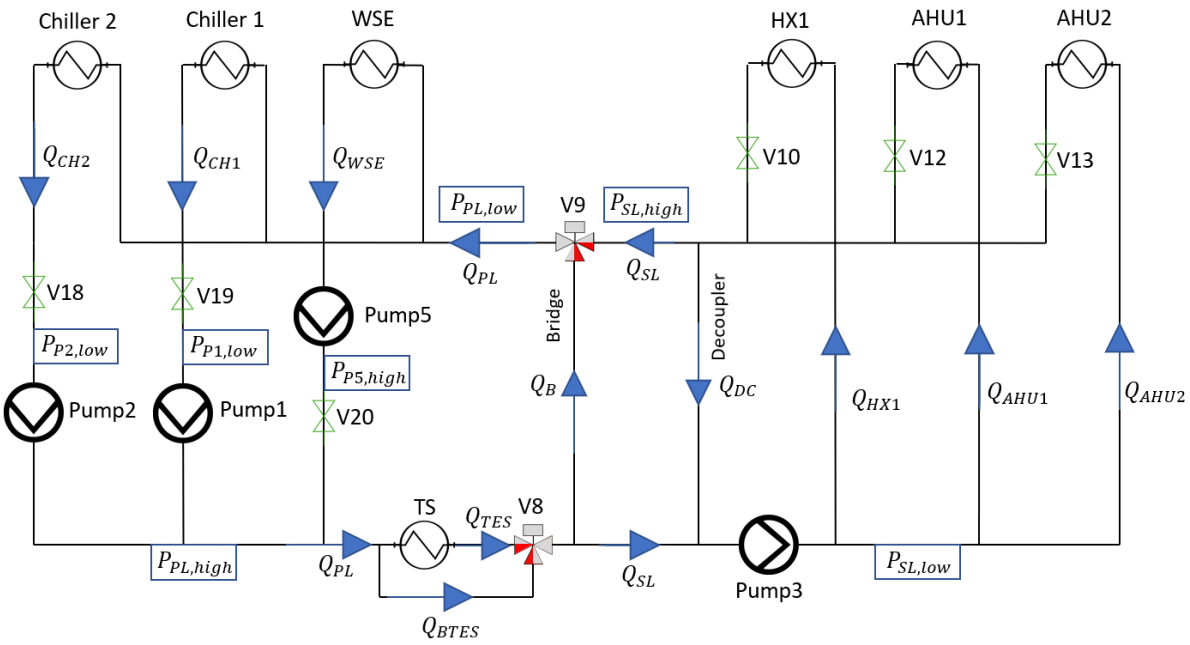

Figure 3.7: Schematic of the hydronic loop illustrating the flow rates that the flow hydraulic calculations Type solves.

The model is formulated as a system of linear equations that are represented in matrix form and then solved using a traditional matrix form method such as Gaussian elimination. This approach yields a model that is fully defined, and that could also be modified to reflect any future changes to the hydronic system's layout. Equations (3.19) to (3.36) represent the system of equations that the model is based on, of which variables are reflected in 5.5. The equations relate the pressures at the branch nodes and include dependence on mass flow to ensure mass conservation.

$$\mathrm{P_{P2,low}} = \mathrm{P_{low}} \tag{3.19}$$

$$\mathrm{P_{P2,low}} = \mathrm{P_{PL,low}} - \mathrm{Q_{CH2}\ R_{V18}} \tag{3.20}$$

$$\mathrm{P_{PL,high}} = \mathrm{P_{P2,low}} + \Delta\ \mathrm{P_{P2}} \tag{3.21}$$

$$\mathrm{P_{P1,low}} = \mathrm{P_{PL,low}} - \mathrm{Q_{C}H1\ R_{V19}} \tag{3.22}$$

$$P_{PL,high} = P_{P1,low} + \Delta P_{P1} \tag{3.23}$$

$$P_{P5,high} = P_{PL,low} + \Delta P_{P5} \tag{3.24}$$

$$P_{PL,high} = P_{P5,high} - Q_{WSE}\ R_{V20} \tag{3.25}$$

$$P_{PL,high} = P_{SL,low} + Q_{TES}\ R_{V8,p} \tag{3.26}$$

$$P_{PL,high} = P_{SL,low} + Q_{BTES}\ R_{V8,s} \tag{3.27}$$

$$P_{SL,high} = P_{SL,low} + \Delta P_{P3} \tag{3.28}$$

$$P_{SL,high} = P_{SL,low} + Q_{AHU2}\ R_{V13} \tag{3.29}$$

$$P_{SL,high} = P_{SL,low} + Q_{AHU1}\ R_{V12} \tag{3.30}$$

$$P_{SL,high} = P_{PL,low} + Q_{HX1}\ R_{V10} \tag{3.31}$$

$$P_{SL,low} = P_{PL,low} + Q_{SL}\ R_{V9,p} \tag{3.32}$$

$$P_{SL,low} = P_{PL,low} + Q_{B}\ R_{V9,s} \tag{3.33}$$

$$Q_{CH2} + Q_{CH1} + Q_{WSE} = Q_{TSE} + Q_{BTSE} \tag{3.34}$$

$$Q_{B} + Q_{SL} = Q_{WSE} + Q_{CH1} + Q_{CH2} \tag{3.35}$$

$$Q_{SL} + Q_{DC} = Q_{HX1} + Q_{AHU1} + Q_{AHU2} \tag{3.36}$$

In order to solve the coefficient matrix for this system of equations, there are multiple methods to find an inverse of a matrix; in this implementation, a subroutine that uses Gaussian elimination is incorporated into the TRNSYS type. Given an initial guess value for a flow rate, the model iterates until it reaches an error value that satisfies a user-specified tolerance.

Pumps and Valves

In order to incorporate the pumps and valves into the model, their pressure characteristic needs to be properly modeled. Pumps are characterized by their pressure rise which is a function of both flow rate and rotational speed, meanwhile, valves are characterized by

their nominal pressure drop which is a function of both nominal flow rate and opening position.

Several characterization tests were performed on the pumps and valves present in the IBAL. The tests were conducted by operating the system while varying a single operating condition (e.g. system restriction) and holding other conditions constant (e.g. pump speed). The tests were performed such that the "head-flow" curves of the pumps could be created. Meanwhile, the nominal flow rate and pressure drop for each valve were approximated due to the lack of pressure sensors at certain locations in the hydronic system.

A similar mapping between pump power consumption and flow rate was developed for the pumps using the data collected at different speeds. In Figure 3.8, the pressure rise for pump 3 (secondary loop pump) is plotted as a function of flow rate at its maximum rotational speed. This curve is relevant as it is normalized by the maximum pressure rise and flow rate values, which results in the curve shown in Figure 3.9. Subsequently, the maximum pressure rises and maximum flow rates are plotted as a function of pump rotational speed in Figure 3.10.

Given a flow rate value F and rotational speed N, the maximum flow rate function is used to compute the normalized flow rate F_{norm} at the given N as shown in Equations 3.37 and 3.38

$$F_{max} = a_0 + a_1 N \tag{3.37}$$

$$F_{norm} = \frac{F}{F_{max}} \tag{3.38}$$

Similarly, Equation 3.39 is used to calculate the maximum pressure rise ΔP_{max}, and Equation 3.40 is used to compute the normalized pressure rise ΔP_{norm}. Finally, the two calculated values are used in Equation 3.41 to compute the denormalized predicted pressure rise ΔP_{pump}.

$$\Delta P_{max} = b_1 N + b_2 N^2 \tag{3.39}$$

$$\Delta P_{norm} = c_0 + c_1 F_{ratio} + c_2 {F_{ratio}}^2 \tag{3.40}$$

$$\Delta P_{pump} = \Delta P_{max} \Delta P_{norm} \tag{3.41}$$

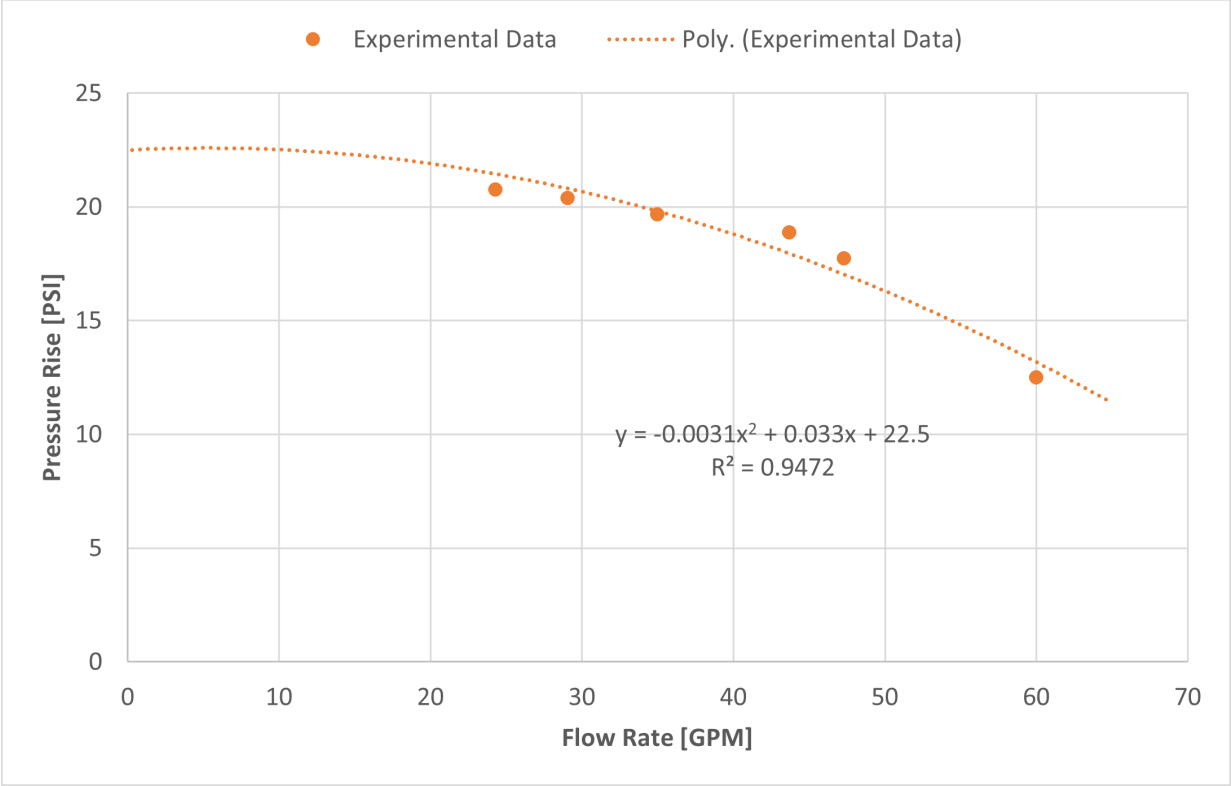

Figure 3.8: Schematic of the hydronic loop illustrating the flow rates that the flow hydraulic calculations Type solves.

Similarly, the pump power can be mapped to the flow rate and normalized as illustrated in Figure 3.11, and the maximum power can be mapped to the pump rotational speed as shown in Figure 3.12. Given a flow rate value F and rotational speed N, the maximum flow rate function is used again to compute the normalized flow rate F_{norm} at a given N as shown in Equations 3.37 and 3.38. Different from before, Equation 3.42 is used to calculate the maximum power consumption $Power_{max}$, and Equation 3.43 is used to compute the normalized pressure rise $Power_{norm}$. Finally, the two computed values are used in

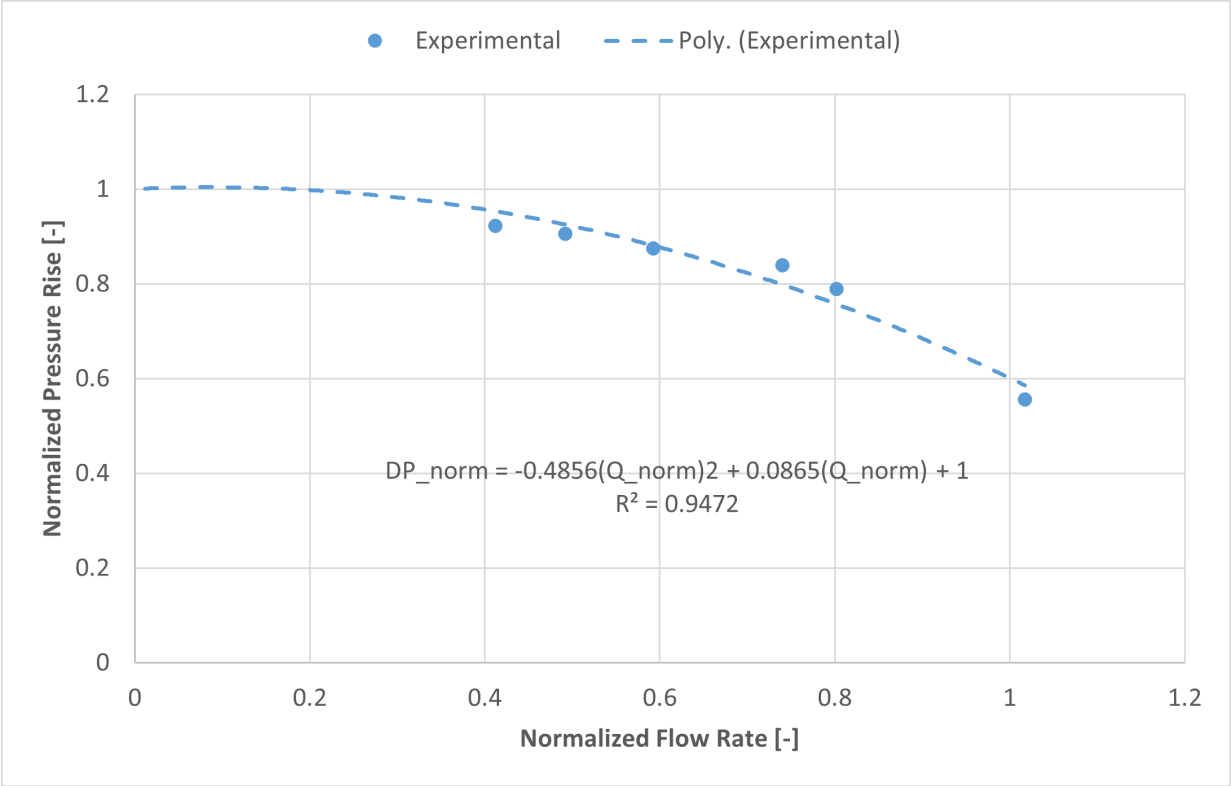

Figure 3.9: Normalized pump head as a function of normalized flow rate for pump 3

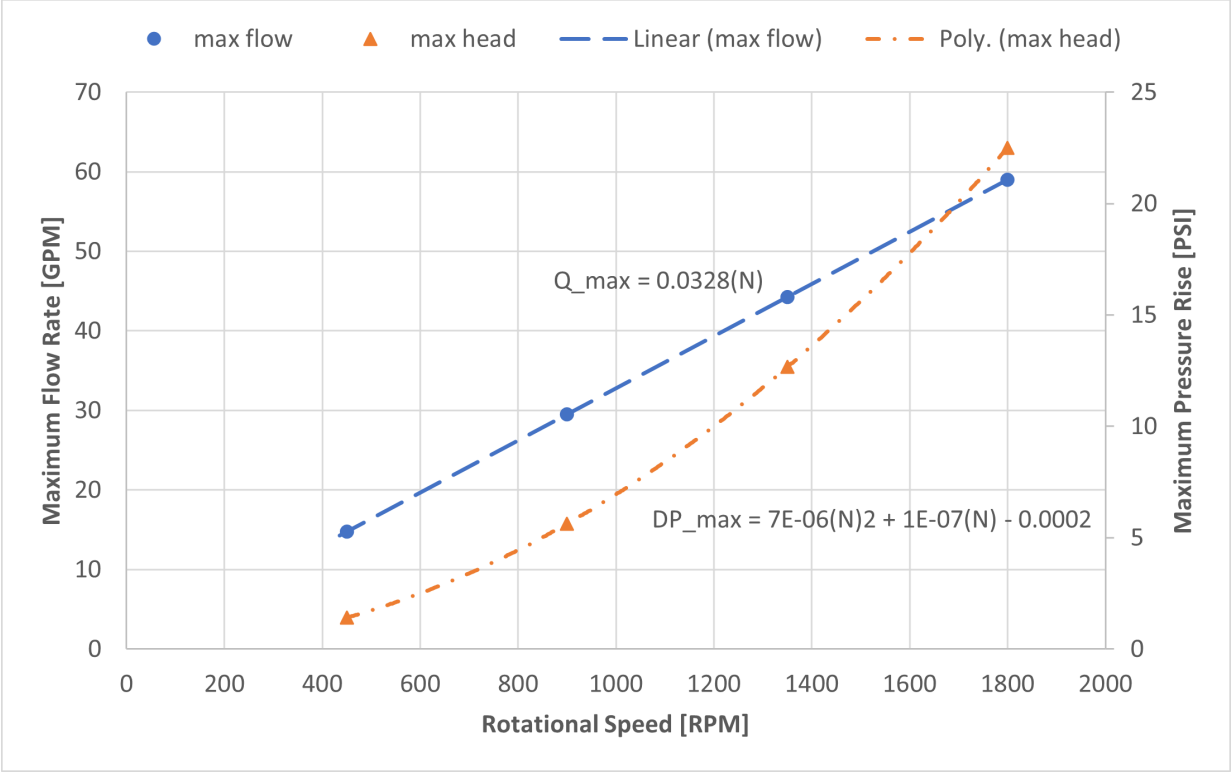

Figure 3.10: Maximum head and flow at a given pump speed for pump 3

Equation 3.44 to return the denormalized predicted power consumption $Power_{pump}$.

$$Power_{max} = d_0 + d_1 N + d_2 N^2 \tag{3.42}$$

$$Power_{norm} = e_0 + e_1 F_{norm} \tag{3.43}$$

$$Power_{pump} = Power_{max} Power_{norm} \tag{3.44}$$

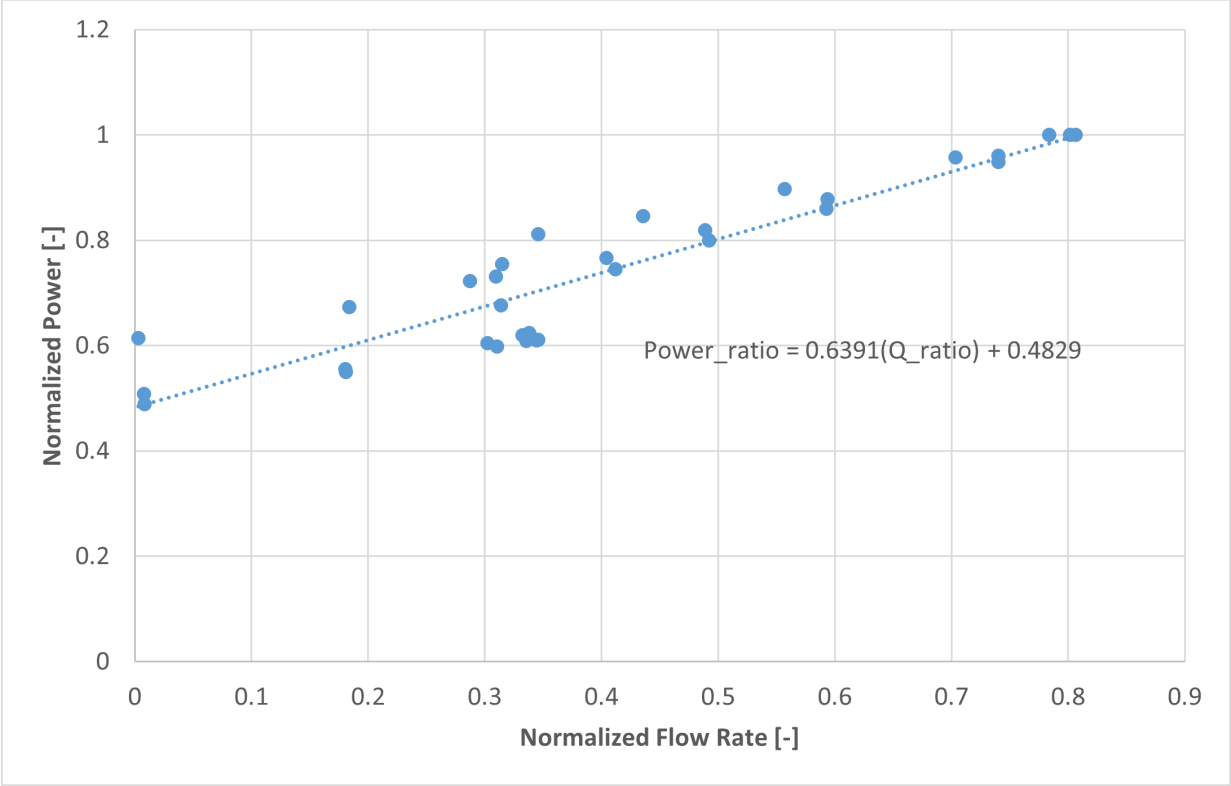

Figure 3.11: Normalized pump power as a function of normalized flow rate for pump 3.

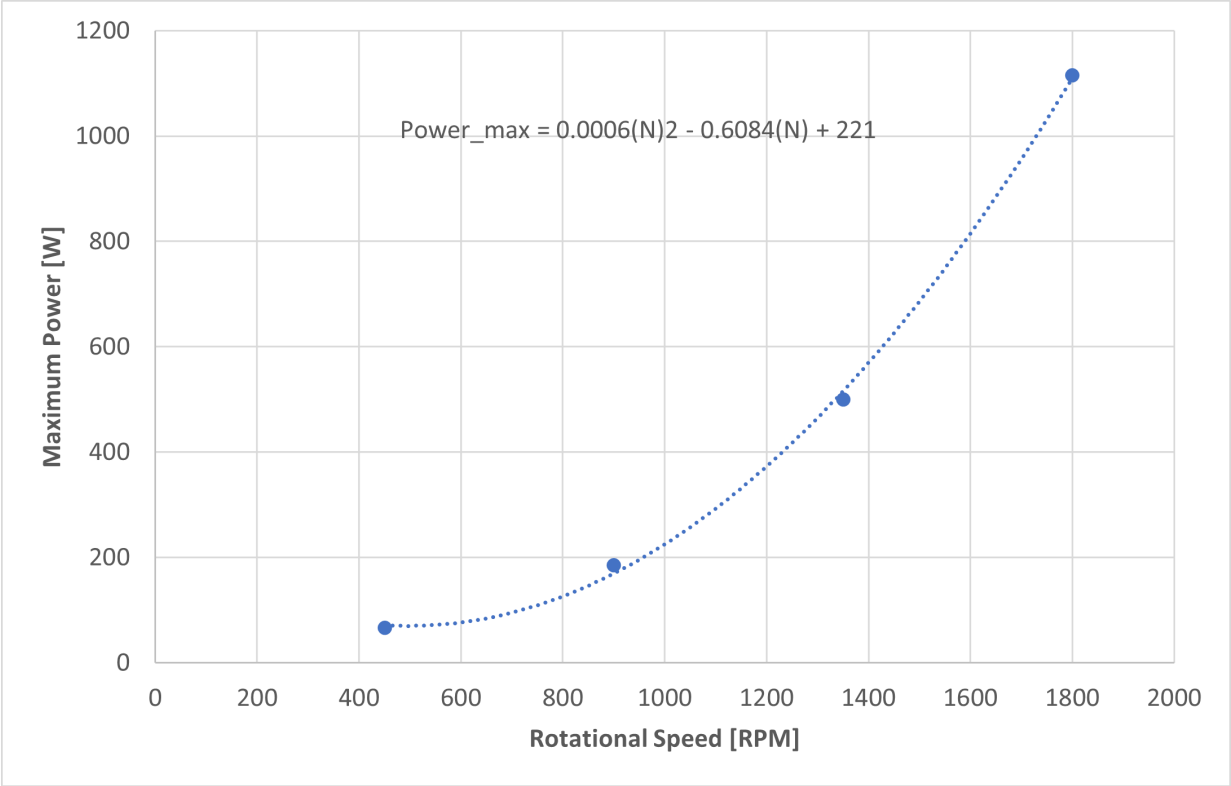

Figure 3.12: Maximum power consumption at a given pump speed for pump 3

4 HYDRONIC SYSTEM CONTROL

HVAC control systems can be divided into two main levels: supervisory and local. The supervisory level is responsible for making high-level decisions, such as selecting the appropriate chiller to meet the building's current load and determining the desired temperature for the chiller's output water. An example of this is the Model Predictive Controller uses optimization techniques for optimal control, which a developed example is presented in this chapter.

4.1 Supervisory Controllers

Hydronic System Control Mode

The purpose of this supervisory controller is to coordinate between two other supervisory controllers that act on the same input; one controller computes the primary loop/chiller setpoint temperature value, and the other calculates the differential pressure setpoint value in the secondary loop, both of which act on the cooling coils valves' positions. The purpose of the cooling coil control valves is to regulate the chilled water flow rate through the hydronic side of the coils based on the "building" side demand.

When the real IBAL first starts, if the cooling load is low (i.e. cooling coils control valves are closed below a specified threshold indicating less cooling is needed), priority is given to the primary loop/chiller temperature setpoint controller such that it increases the setpoint until a maximum value is reached. The reasoning behind this is that adjusting the chiller/primary loop's temperature setpoint (which decides the chiller's setpoint temperature) has a greater impact on energy consumption than adjusting the secondary loop pump pressure setpoint, therefore, it is more sensible to prioritize.

If the cooling load continues to decrease and the chiller/primary loop temperature

setpoint is saturated at its maximum value, the secondary loop differential pressure is decreased. In response, this results in the secondary loop pump reducing its speed using a proportional local controller, which reduces the chilled water flow rate to the cooling coils. Figure 4.1 illustrates the process of this coordinated process between the two supervisory controllers.

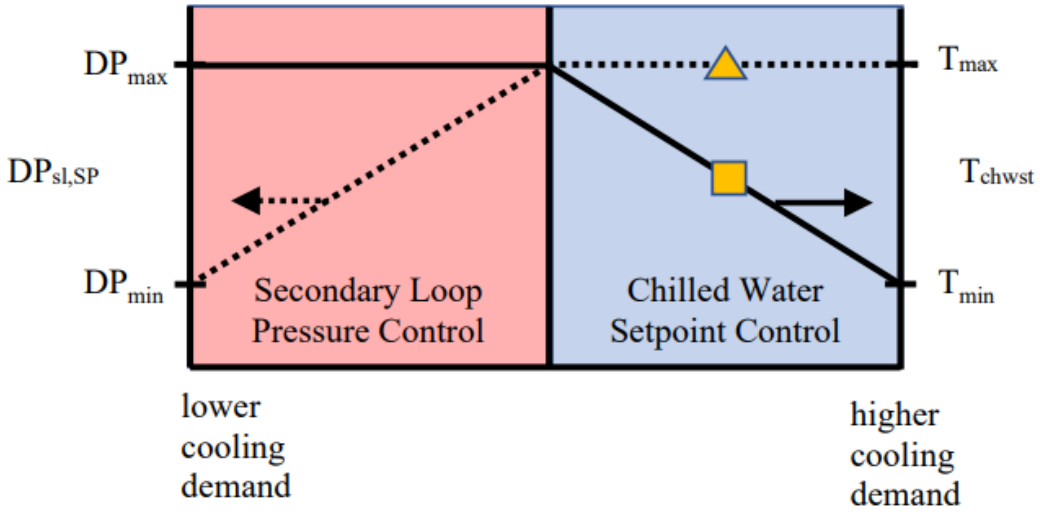

Figure 4.1: A pictorial representation of the supervisory controllers responsible for regulating the hydronic system's response to "building" load. The solid line represents the setpoint temperature while the dotted line represents the differential pressure setpoint

The hydronic loop algorithm decides which hydronic control mode (i.e. supervisory controller) to engage. As shown in the pseudo-code presented in Algorithm 1, when the system is first turned on, it checks what the primary mode is. For instance, if the primary mode is ice-making, then that engages the temperature setpoint controller in ice-making mode. The operational modes are further discussed in detail in Chapter 5. These checks are performed because each primary mode can require a special signal sent to the setpoint temperature controller. Once the algorithm goes through the checks, it checks whether the current setpoint temperature is less than the maximum setpoint value. If true, then it engages the temperature setpoint controller. If it is not true (i.e. setpoint temperature is maxed), then it engages the differential pressure setpoint controller.

Algorithm 1 Determine the mode of the hydronic system

```
if Pmode == MakeIce then
    mode = CHWST-Make Ice
else if Pmode == SimDischarge then
    mode = CHWST-Discharge Ice and Chiller
else if Pmode == MakeIceAndMeetLoad then
    mode = CHWST- Make Ice and Meet Load
else
    if chMode == Auto & dpMode == Auto then
        if T_chwst < T_max then
            mode = CHWST                          ▷ the mode is CHWST
        else
            mode = DP                             ▷ the mode is DP
        end if
    else if chMode == Auto & dpMode == Manual then
        mode = CHWST
    else
        mode = DP
    end if
end if
return mode
```

Table 4.1 documents the inputs, outputs, and parameters associated with the TRNSYS model.

Table 4.1: Inputs, outputs, and parameters for TRNSYS Type 9001—the hydronic system control model.

Symbol	Units	Default	Description
Parameters			
chMode	–	1	0: Manually set the setpoint. 1: Automatically set the setpoint
dpMode	–	1	0: Manually set the setpoint. 1: Automatically set the setpoint
T_{min}	°C	4.4	Minimum chiller setpoint
T_{max}	°C	21.1	Maximum chiller setpoint
Inputs			
PMode	–	3	Primary mode of the system
T_{chwsp}	°C	10	Chiller setpoint temperature
Outputs			
mode	–	–	Mode signal that determines which controller to activate

Primary Loop/Chiller Temperature Setpoint

The primary loop/chiller temperature setpoint controller is driven by the cooling coils' valve positions. The controller is modified from the actual IBAL such that it also sets the outlet temperature of the primary loop. The chiller setpoint temperature is equal to the primary loop setpoint temperature if the chiller is meeting demand on its own. Otherwise, it will depend on whether ice is being made in the TES or if the chiller is used in conjunction with the TES to meet demand. In the latter case, the temperature drop required to achieve the primary loop outlet temperature is divided between the TES and the chiller, according to a specified fraction. The pseudo-code for this controller is presented in Algorithm 2.

If the average value of either valve position is greater than a high threshold (indicating more "building" load) over a number of time steps, then the primary loop temperature is reduced. Otherwise, the temperature setpoint is increased. Once that value is computed, the setpoint temperature of the chiller is set based on the primary mode the system is in.

Table 4.2 documents the inputs, outputs, and parameters associated with the TRNSYS model.

Algorithm 2 Determine the chiller and primary loop setpoint temperature

first call: $N = 0; v12Sum = 0; v13Sum = 0; T_{chwst} = SP0$
if $mode \neq DP$ **then**
  N = N + 1
  v12Sum = v12Sum + v12
  v13Sum = v13Sum + v13
  if N>n **then**
    if $((v12Sum/N)$ or $(v13Sum/N)) > high$ **then**
      $T_{PL,out,sp} = T_{PL,out,sp} - \Delta$
    else if $((v12Sum/N)$ or $(v13Sum/N)) < low$ **then**
      $T_{PL,out,sp} = T_{PL,out,sp} + \Delta$
    end if
    N = 0
    v12Sum = 0
    v13Sum = 0
  end if
  $T_{PL,out,sp} = max(min(T_{PL,out,sp}, T_{max}), T_{min})$
  $T_{chwst} = T_{PL,out,sp}$
  $dT = max(0.0,\ T_{chw,in} - T_{chwst})$
  if $mode == MakeIce$ **then**
    $T_{chwst} = T_{makeice}$
    $T_{PL,out,sp} = CloseBridgeValve$
  else if $mode == SimDischarge$ **then**
    $T_{chwst} = T_{PL,out,sp} + (1 - dT_{frac} * dT)$
  else if $Pmode == MakeIceAndMeetLoad$ **then**
    $T_{chwst} = T_{makeice}$
  end if
end if
return $T_{PL,out,sp}, T_{chwst}$

Table 4.2: Inputs, outputs, and parameters for TRNSYS Type 9002—the primary loop/chiller temperature setpoint control model.

Symbol	Units	Default	Description
Parameters			
n	–	72	Number of time steps between setpoint changes
$high$	–	0.6	Threshold to indicate that the valves are open, indicating more cooling is needed
low	–	0.3	Threshold to indicate that the valves are closed, indicating less cooling is needed
T_{min}	°C	4.4	Minimum chiller setpoint
T_{max}	°C	21.1	Maximum chiller setpoint
Δ	°C	0.28	The amount by which to change the SP
$SP0$	°C	10	Default setpoint; when the system is off it will go to this SP and when it turns on it will start from this setpoint
$T_{makeice}$	°C	-3.3	Ice-making temperature setpoint
Inputs			
$PMode$	–	3	Primary mode of the system
$T_{chw,in}$	°C	10	Chiller inlet temperature
dT	°C	0.5	Fraction of the temperature drop required that the Chiller achieves
$v12$	–	0.8	Position of the valve in the cooling coil in AHU1
$v13$	–	0.8	Position of the valve in the cooling coil in AHU2
Outputs			
T_{chwsp}	°C	–	Chiller setpoint temperature
$T_{PL,out,sp}$	°C	–	Primary loop setpoint temperature

Secondary Loop Differential Pressure Setpoint

Similarly, the secondary loop differential pressure setpoint controller is driven by the cooling coils' valve positions. The pseudo-code for this controller is presented in Algorithm 3, which is slightly simpler than the previous controller. In this case, the only mode where the secondary loop is not operating (i.e. pump is off) is during ice-making mode without any "building" demand from the air system. Using the same thought process, if the average value of either valve position is greater than a high threshold (indicating more "building" load) over a number of time steps, then the secondary loop differential pressure is increased (which increases the flow rate). Otherwise, the differential pressure setpoint is decreased.

Algorithm 3 Determine the pressure differential setpoint for the secondary loop pump

first call: $N = 0; v12Sum = 0; v13Sum = 0; DP_{sl,SP} = SP0$
if $mode == DP$ **then**
  N = N + 1
  v12Sum = v12Sum + v12
  v13Sum = v13Sum + v13
  if N>n **then**
    if $((v12Sum/N)$ or $(v13Sum/N)) > high$ **then**
      $DP_{sl,SP} = DP_{sl,DP} + \Delta$
    else if $((v12Sum/N)$ or $(v13Sum/N)) < low$ **then**
      $DP_{sl,SP} = DP_{sl,SP} - \Delta$
    end if
    N = 0
    v12Sum = 0
    v13Sum = 0
  end if
  $DP_{sl,SP} = max(min(DP_{sl,SP}, DP_{max}), DP_{min})$
else if $mode == MakeIce$ **then**
  $DP_{sl,SP} = 0.0$
end if
return $DP_{sl,SP}$

Table 4.3 documents the inputs, outputs, and parameters associated with the TRNSYS model.

Table 4.3: Inputs, outputs, and parameters for TRNSYS Type 9003—the secondary loop differential pressure setpoint control model.

Symbol	Units	Default	Description
Parameters			
n	–	72	Number of time steps between setpoint changes
$high$	–	0.6	Threshold to indicate that the valves are open, indicating more cooling is needed
low	–	0.3	Threshold to indicate that the valves are closed, indicating less cooling is needed
DP_{min}	PSI	2	Minimum value of the setpoint
DP_{max}	PSI	55	Maximum value of the setpoint
Δ	PSI	0.28	The amount by which to change the SP
SP0	PSI	55	Default setpoint; when the system is off it will go to this SP and when it turns on it will start from this setpoint
Inputs			
PMode	–	3	Primary mode of the system
$v12$	–	0.8	Position of the valve in the cooling coil in AHU1
$v13$	–	0.8	Position of the valve in the cooling coil in AHU2
Outputs			
DP_{SL}	PSI	–	Differential pressure setpoint

4.2 Model Predictive Controller

Model Predictive Control (MPC) stands as an optimization-based control algorithm, leveraging a defined model of the system to generate optimal control decisions. At its core, MPC predicts the future system states based on the model's dynamics and employs the prediction to minimize a mathematical cost function, across a predetermined finite time horizon as illustrated in Figure 4.2. The optimization task aims to find the optimal sequence of control inputs that not only drive the system toward desired states but also adhere to constraints and handle disturbances. This approach, in essence, entails formulating and solving a constrained optimization problem in a receding horizon framework.

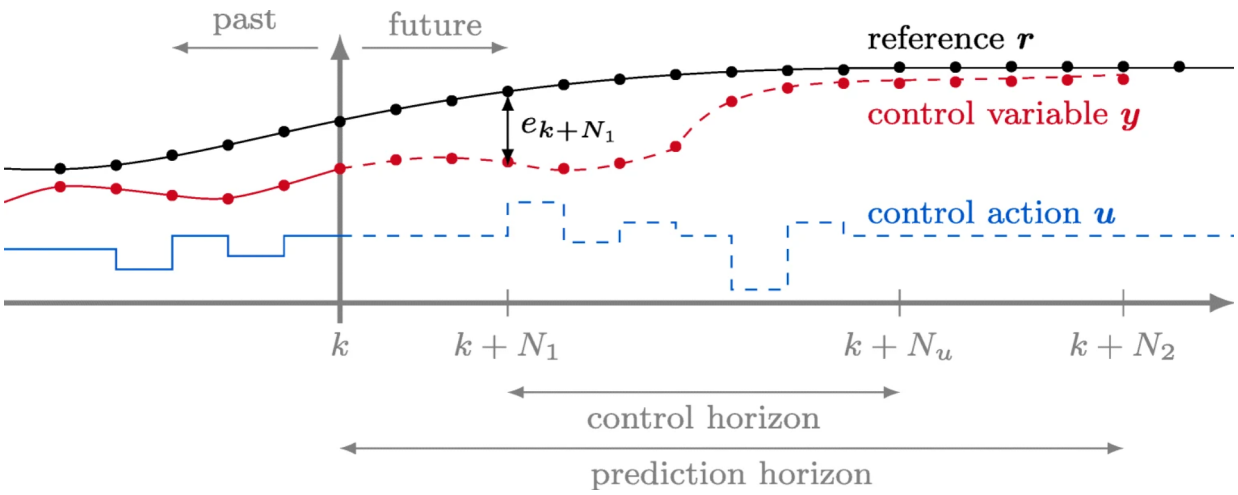

Figure 4.2: A visualization of a model predictive controller responding as a function of time [1]

Despite the computational intricacies tied to solving such problems repeatedly, the advancement in optimization techniques and computational resources has facilitated the real-time implementation of MPC in various complex systems, including those with nonlinear dynamics and intricate constraints. Examples of MPC applications can be found in industries such as chemical processing, power electronics, autonomous vehicles, and building climate and energy [1]. Based on the work done in building energy optimization [11][12], MPC has shown promise in effectively integrating energy storage components to minimize building energy costs while maintaining thermal comfort.

For that reason, an MPC is developed to generate optimal control actions for the IBAL's chiller plant, specifically leveraging thermal energy storage. Based on the work done by [13], first, a model for the system's dynamics and economics is developed. In this case, the dynamics model captures the physics of chilling components, and the economics model captures the cost of operating the system in terms of power consumption cost and defined penalties for specific actions.

The chiller plant model contains one chiller that can operate in either an "ice making" or "load meeting" mode, as well as an ice thermal energy storage that can be charged and meet the load. The building load demand and the equipment energy consumption

are modeled as inputs for the MPC, while the equipment's specification is provided as parameters. The chiller is modeled assuming constant operating conditions (i.e. constant T_{cw} and $T_{chw,sp}$) with load-dependant COP and ramping limits. Meanwhile, the thermal energy storage is modeled as a simple energy kWh counter with both storage and heat exchange efficiencies. Given these assumptions, the dynamics of the model are considered to be linear at each time step.

Model Description

The architecture of the system modeled consists of the following components: a chiller, a thermal energy storage, and a building load demand. The dynamics of the system are defined with a state variable $\mathbf{x}(t) \in \mathbf{R}^n$ that varies over time steps $t = 0, \ldots, T$, where T is the prediction time horizon (same as optimization period). $\mathbf{u}(t) \in \mathbf{R}^m$ denotes the control variable that is manipulated at each time step to influence the system's state. Given these definitions, $\mathbf{x}(t)$ represents the state of the TES and the building load demand, while $\mathbf{u}(t)$ represents the power allocation of each chilling resource.

The variable $x_1(t)$ denotes the state of charge (SOC) of the thermal energy storage (kWh_{th}), which is bounded by $[\bar{x}_{1,min}, \bar{x}_{1,max}]$. The variable $x_2(t)$ denotes the cooling deficit/surplus of the building (kWh_{th}), where a positive value means a cooling deficit and a negative value means a cooling surplus. For the action variables, $u_1(t)$ denotes the chiller power allocated to charge the thermal energy storage (kW), bounded by $[0, \bar{u}_1]$. The variable $u_2(t)$ denotes the cooling demand met by the thermal energy storage (kW_{th}), bounded by $[0, \bar{u}_2]$. The variable $u_3(t)$ denotes the power allocated to the chiller to meet cooling demand directly (kW), bounded by $[0, \bar{u}_3]$. The building cooling demand (kW_{th}) is defined as $w_1(t)$, and the building's lighting and equipment electricity consumption (kW) is defined as $w_2(t)$.

The rate at which the control variable $\mathbf{u}(t)$ can change is constrained by ramping

limits for each resource; the control variable from the previous time step $\mathbf{u}(t-1)$ is appended to the current state variable $\mathbf{x}(t)$, which redefines the state variable as $\mathbf{x}(t) = \begin{bmatrix} x_1(t) & x_2(t) & \mathbf{u}(k-1) \end{bmatrix}$. In order to enforce a single-mode system operation at each time step (i.e. only one control variable $u_i(t)$ is nonzero), a binary variable $\mathbf{z}(t)$ is defined. The binary variable $\mathbf{z}(t)$ is appended to the lower and upper bounds of the control variable $\mathbf{u}(t)$. By constraining the sum of $\mathbf{z}(t)$ to unity, it enforces that only one binary variable is non-zero, thus, only one control variable is non-zero.

As a result, this leads to a state variable constrained as $\mathbf{x}(t) \in \mathcal{X} = [0, \bar{x}_{1,max}] \times \mathbf{R}^{n+m}$, a control variable constrained as $\mathbf{u}(t) \in \mathcal{U}(\mathbf{x}(t), \mathbf{z}(t)) = \left\{ \mathbf{u} \in \mathbf{R}^m \middle| u_i \in [0, \bar{u}_i \cdot z_i], |u_i - x_{i+2}(t)| \leqslant \Delta \bar{u}_i \right\}$, and a binary variable constrained as $\mathbf{z}(t) \in \mathcal{Z} = \left\{ \mathbf{z} \in \mathbf{R}^m \middle| \sum_{i=1}^{m} z_i = 1 \right\}$. Each system state dynamics can be expanded in Equations 4.1 through 4.3

$$x_1(t+1) = \eta_{ret} x_1(t) + COP_{ice} u_1(t) \Delta t - u_2(t) \Delta t / \eta_{melt} \tag{4.1}$$

$$x_2(t+1) = x_2(t) + [w_1(t) - u_2(t) - COP_{nom}(t) u_3(t)] \Delta t \tag{4.2}$$

$$x_i(t+1) = u_{i-2}(t), i \in \{3, 4, 5\} \tag{4.3}$$

where η_{ret} is the TES ice retention efficiency that depends on how well the tank is insulated and can hold charge, COP_{ice} is the chiller's coefficient of performance during the ice-making mode, and COP_{nom} is the chiller's coefficient of performance during the direct load-meeting mode. It is worth emphasizing that COP_{nom} is demand-dependent, which in this case is time-dependent, thus, making it a time-varying value. This value is computed for each time step based on the predicted load w_1. The system's dynamics can be represented in a more concise manner as shown in Equation 4.4

$$\mathbf{x}(t+1) = A\mathbf{x}(t) + B(t)\mathbf{u}(t) + G\mathbf{w}(t) \tag{4.4}$$

where $A \in \mathbf{R}^{n \times n}$ and $B \in \mathbf{R}^{n \times m}$ and $G \in \mathbf{R}^{n \times m}$ are known matrices. The goal is to find the optimal control actions $u_0, \ldots, u_{T-1}$ that minimize a cost function. The cost function is defined in two terms: a net period cost $\ell_t(t)$ and a terminal cost ℓ_T. The net period cost is defined as the cost of energy consumption, a quadratic penalty cost for meeting the building load demand imperfectly (either by over-cooling or under-cooling) over the optimization period, and a penalty cost that discourages mode switching between subsequent time steps using a tunable parameter, all of which are represented in Equation 4.5

$$\ell_t(\mathbf{x}_t, \mathbf{u}_t, \mathbf{w}_t, \mathbf{z}_t) = c_e(t)p(t)\Delta t + c_u(t)x_2(t)^2 + c_m|z(t+1) - z(t)| \tag{4.5}$$

where $p(t) = u_1(t) + u_3(t) + w_2(t)$ in (kW), $c_e(t)$ is the monetary cost of energy in $(\$/kWh)$, $c_u(t)$ is a cooling deviation penalty parameter that is set proportional to the building load, and lastly c_m is a tunable penalty parameter for mode switching. On the other hand, the terminal cost is defined as a penalty cost for the TES final SOC relative to its initial value; this discourages complete tank depletion by the end of the optimization period as defined in Equation 4.6

$$\ell_T(\mathbf{x}_T) = c_{td}(x_1(0) - x_1(T))^+ \tag{4.6}$$

where c_{td} is a tunable penalty parameter, and $(\cdot)^+$ denotes the positive part of the difference term such that only storage depletion is discouraged rather than storage filling as

well. The optimization problem can be summarized in Equations 4.7 through 4.11

$$\text{minimize} \sum_{t=0}^{T-1} \ell_t(x_t, u_t, w_t, z_t) + \ell_T(x_T) \tag{4.7}$$

$$\text{subject to } \mathbf{x}(t+1) = A\mathbf{x}(t) + B(t)\mathbf{u}(t) + G\mathbf{w}(t), \quad t = 0, \ldots, T-1 \tag{4.8}$$

$$\mathbf{x(t+1)} \in \mathcal{X} \tag{4.9}$$

$$\mathbf{u(t+1)} \in \mathcal{U}(\mathbf{x}_t, \mathbf{z}_t) \tag{4.10}$$

$$\mathbf{z(t+1)} \in \mathcal{Z} \tag{4.11}$$

4.3 Local Controllers

On the other hand, the local control level focuses on managing individual processes or actions based on the system's state relative to a reference value. As an example, a valve might be adjusted to regulate a temperature relative to a setpoint value provided by the supervisory level. A local control loop mainly consists of four parts:

1. A process that is controlled
2. A measurement of the process state
3. A controller that outputs a control decision based on the current process state and the desired process state
4. An actuator that converts the control decision into a change in physical state

The IBAL system employs multiple local control loops; these control loops implement conventional proportional-integral-derivative (PID) controllers. Moreover, these controllers are implemented for various processes in the hydronic system, such as controlling the secondary loop entering temperature, the primary loop leaving temperature, and the cooling coils air off temperature.

Primary Loop Outlet Temperature

The primary loop outlet temperature is driven by the setpoint temperature of the chiller that is operating, in which case, the mixing valve shown in Figure 4.3 bypasses the TES completely. However, if the TES is also operating, then the mixing valve is modulated to achieve the desired primary loop outlet temperature. Figure 4.3 identifies the main parts of this local control loop. In this case, the control process is the primary loop outlet temperature, which is measured at the outlet of the primary loop after the ice tank. The control decision is the mixing valve position, while the setpoint value is provided by the primary loop setpoint temperature supervisory controller.

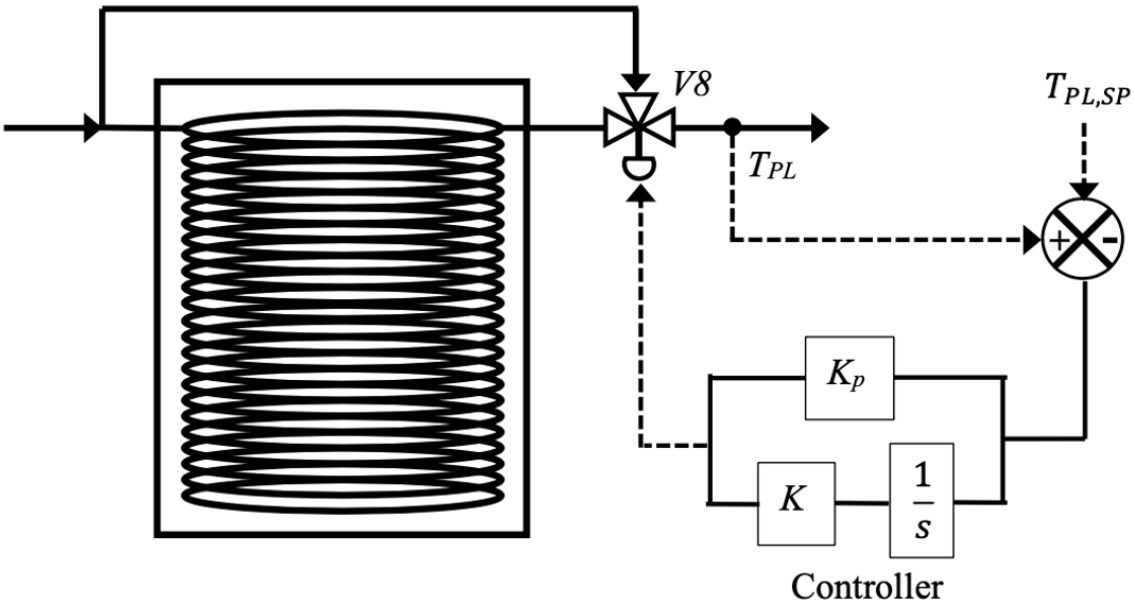

Figure 4.3: The local PI control loop for the TES valve position which regulates the primary loop outlet temperature

Secondary Loop Inlet Temperature

The secondary loop inlet temperature can be regulated by adjusting the mixing valve located in the bridge piping between the primary and secondary loops. The main purpose of the bridge is to hydraulically separate the two loops, allowing them to have different

temperatures and flow rates. The ability to control the temperature is useful in cases where the TES is operating. For instance, if the TES is being charged with ice and a building load is present, the mixing valve can be modulated such that it maintains a specific chilled water supply temperature to the cooling coils. As of now, the real IBAL calculates the secondary loop setpoint temperature either manually or as a constant offset from the primary loop setpoint temperature. Figure 4.4 shows the main parts of this local control loop. In this case, the control process is the secondary loop inlet temperature, which is measured at the inlet of the secondary loop after the bridge.

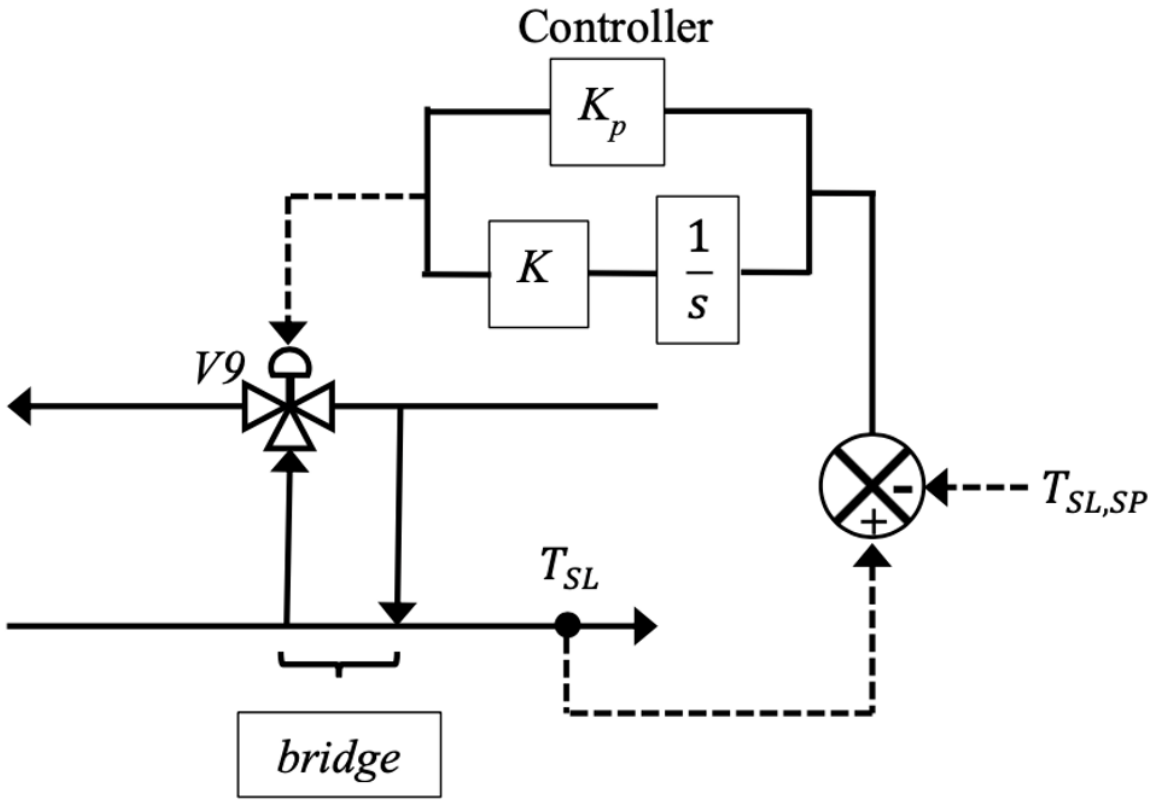

Figure 4.4: The local PI control loop for the bridge valve position which regulates the secondary loop inlet temperature

Cooling Coil Supply Air Temperature

The temperature of the supply air that leaves the AHU is mainly impacted by the chilled water flow rate through the cooling coils, which is regulated by the cooling coil valve

position. By opening the valve and allowing greater chilled water flow through, the air supply temperature would decrease, and vice versa. Figure 4.5 illustrates the main parts of this local control loop. In this case, the control process is the AHU supply air temperature, which is measured at the inlet of the VAV boxes. The supply air temperature setpoint value is provided as a constant value. However, a supply air temperature reset supervisory controller does exist in the real IBAL that could be implemented in TRNSYS, but it was deemed as a possible future addition to the model.

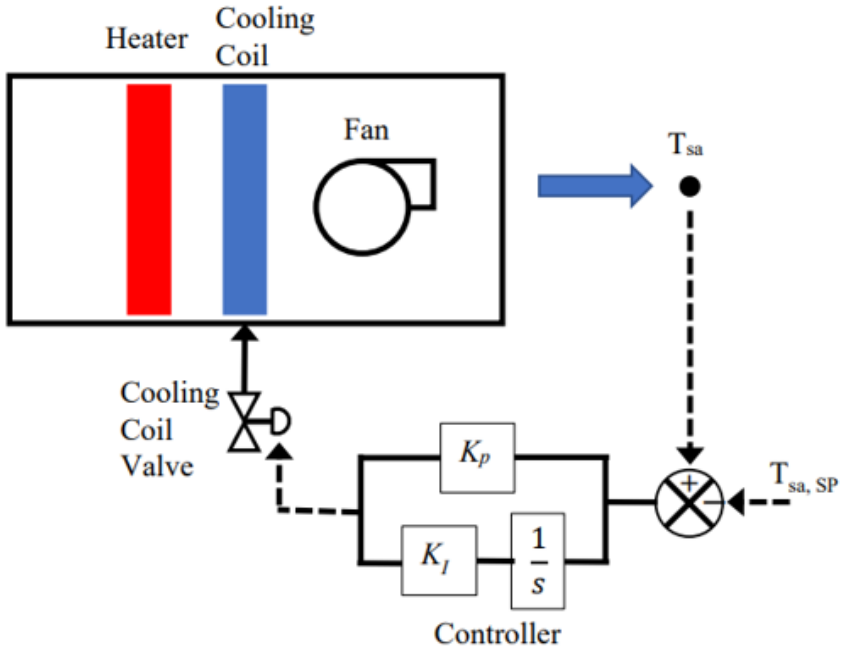

Figure 4.5: The local PI control loop for the cooling coil valve position which regulates the AHU supply air temperature

5 COMPLETE IBAL MODEL

The primary focus of this project is to develop a comprehensive and holistic model of the IBAL in TRNSYS; this model should be capable of simulating the IBAL in its different operational modes (e.g. meeting load, charging TES, etc). Through previous work done by [2], models for the air side system were developed and validated to ensure an appropriate level of fidelity. This chapter demonstrates the integration of the hydronic system with the air side system and showcases the operational modes and the user interface.

In terms of the similarity of the TRNSYS model to the IBAL layout, it is deemed sufficient to include one air handling unit (AHU2) in the model; this allows for more convenient model troubleshooting and experimentation. Given how modular TRNSYS is, the addition of the second air handling unit is a simple process once it is deemed suitable. All other IBAL components are included in the TRNSYS simulation.

5.1 Model Integration

In the IBAL, the hydronic system interacts with the air side system via the cooling coils located in the air handling units. The cooling coils serve as a heat exchanger between the air side air stream and the hydronic side chilled water in order to regulate the temperature of the air stream delivered to the variable air volume boxes.

In TRNSYS, the coupling takes the form of connecting the chilled water flow rate and temperature of the cooling coil model to the chilled water temperature and flow rate inputs. Once done, the air side system can exchange heat with the hydronic side system as designed. As a result, the local controllers are tuned such that the simulations are stable in each of the IBAL operational modes.

5.2 Operation Modes

Since the IBAL contains other chilling components in the primary loop that could meet the load either solely or combined, this results in having multiple possible operational modes. For instance, one of the chillers could be used to meet the load directly, or the ice tank could be used to accomplish that instead. The ice tank could also be charged by one of the chillers, but a cooling demand might be present at the same time; this means that the system has to meet the cooling load and charge the ice tank at the same tank.

Since the chillers are configured in parallel, one assumed limitation in the IBAL is that only one chiller can be operated at a given time; this is because simultaneous operation leads to individual water flow rates below the chiller's minimum flow rates. Consequently, each mode discussed can be accomplished using either chiller. Given the layout and configuration of the IBAL captured in the TRNSYS deck, the main IBAL modes are denoted as primary modes and the chiller choice is denoted as secondary modes. The possible primary operational modes can be summarized as follows:

- Primary Mode 1: Meet a cooling load using the TES
- Primary Mode 2: Charge the TES with ice while no load in the secondary loop
- Primary Mode 3: Meet a cooling load in the secondary loop using a chiller
- Primary Mode 4: Meet a cooling using a chiller and the TES
- Primary Mode 5: Charge the TES with ice and meet a load in the secondary loop

In order to switch between the different modes seamlessly, each IBAL component needs to receive a corresponding signal(s) that sets up the component appropriately. In this case, there is a hierarchy in the manner that these signals propagate throughout the system. During each time step of the simulation, the model requires the primary

and secondary modes as inputs. The provided mode is then passed to a set of logical equations that calculate the relevant signal to the chillers, TES, valves, and pumps in the hydronic system. The logic for the signal is provided in Algorithm 4

Given the set of logic presented in 4, Table 5.1 shows the primary modes with the associated signals for the main components that dictate the operation of each mode. It is worth noting that the secondary modes are not presented since the primary modes can be executed identically with either secondary mode. The relevant parameters that depend on the secondary mode are the chiller signal, the chiller valve, and the chiller pump.

Table 5.1: The primary mode signals for the IBAL based on the mode algorithm presented

Mode	Chiller Signal	Chiller Valve	Chiller Pump	Bridge Valve	TES Valve
1	0	1	1	1	1
2	1	1	1	0	1
3	1	1	1	1	0
4	1	1	1	1	1
5	1	1	1	1	1

The binary signals presented in Table 5.1 can indicate either a signal that is directly sent to a component (e.g. a chiller on/off signal), or a signal sent to a controller that executes the appropriate action based on the primary mode (e.g. fully closing the bridge valve or modulating with PID controller). This explains the reason why although several modes share the same signals, the system response will be different because the primary mode itself is considered a non-binary signal sent to the components to determine its operation.

5.3 User Interface

In order to run a simulation, the user needs to provide the operational mode of the IBAL at each time step. In the TRNSYS deck, the modes can either be manually inputted if a specific mode is run for the entire simulation, or provided in the form of an external text

Algorithm 4 Determine the signals for the hydronic system components based on the operational mode

```
if Pmode ≠ MakeIce then
    V9 = Valve PID On
else
    V9 = Valve PID Off and bypass secondary loop
end if
if (Pmode == MakeIce or MakeIceAndMeetLoad) then
    V8 = Valve fully open to TES
else if Pmode == DichargeChiller then
    V8 = Valve Bypass TES
else
    V8 = Valve PID On
end if
if Smode == CH1 then
    V18 = Close
    V19 = Open
    Pump2 = Off
    Pump1 = On
    if Pmode == DischargeChiller then
        CH1 = On
        CH2 = Off
    else
        CH1 = Off
        CH2 = Off
    end if
else
    V18 = Open
    V19 = Close
    Pump2 = On
    Pump1 = Off
    if Pmode == DischargeChiller then
        CH1 = Off
        CH2 = On
    else
        CH1 = Off
        CH2 = Off
    end if
end if
```

file containing the primary and secondary modes at each time step. This format makes it convenient for an external tool (e.g. a Python script) to generate a schedule of the modes externally.

The complete TRNSYS model is demonstrated with a test case where the model is run on a two-week worth of weather data at Madison, WI. Occupancy count data was also obtained for a large office building; this data is converted into occupant loads in [kW] that are provided to the zone simulator models in TRNSYS. As a summary of the inputs, the user will need to provide the weather data that includes the dry bulb temperature [C] and humidity ratio [-], the occupancy data in the form of energy loads [kW] and humidity gains [kg/hr], the initial SOC of the TES [-], and the primary and secondary mode(s) [-] of the system at each time step.

Case 1: Single-mode simulation

In this case, a singular primary and secondary mode is provided as input prior to the simulation, and the simulation is executed to simulate a 24-hour period. The weather data provided is for a June summer day in Madison, WI. The occupancy information is taken from a three-year dataset for supporting building energy research [14]. The dataset contains metrics such as HVAC operation data, whole-building energy consumption, and occupancy counts. The occupancy count is converted into thermal load given that an average single occupant adds approximately 135W of heat to the occupied environment.

Primary Mode 1: Meet a cooling load using the TES

In this example, the IBAL is simulated to meet the zones' demands using the TES exclusively. Figure 5.1 shows the outdoor temperature condition, as well as the zone temperatures and occupant loads. Since the TES is used to meet the cooling demand, Figure 5.2 illustrates the state of the TES throughout this process.

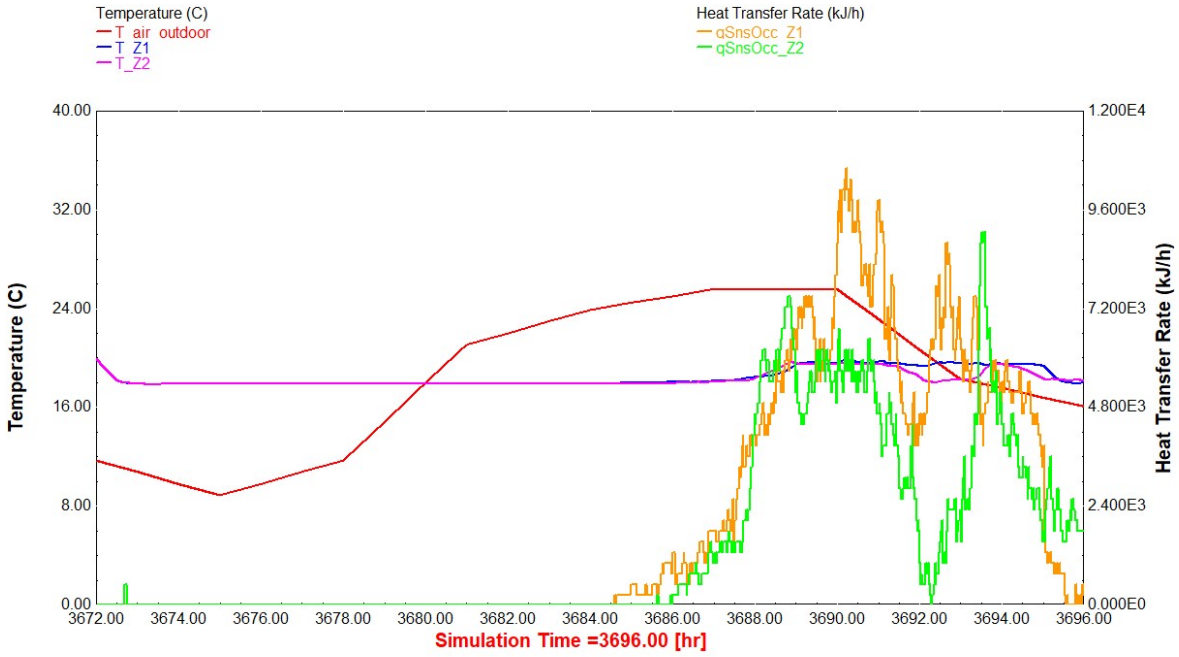

Figure 5.1: On the left axis, the outdoor air temperature $T_{air,outdoor}$ and the respective zone temperatures T_{Z1} and T_{Z2} are plotted. The zones are maintained at a setpoint temperature of 19C. On the right axis, the zones' sensible loads ($qSnsOcc_{Z1}$ and $qSnsOcc_{Z2}$) are plotted indicating the presence of occupants in the zones

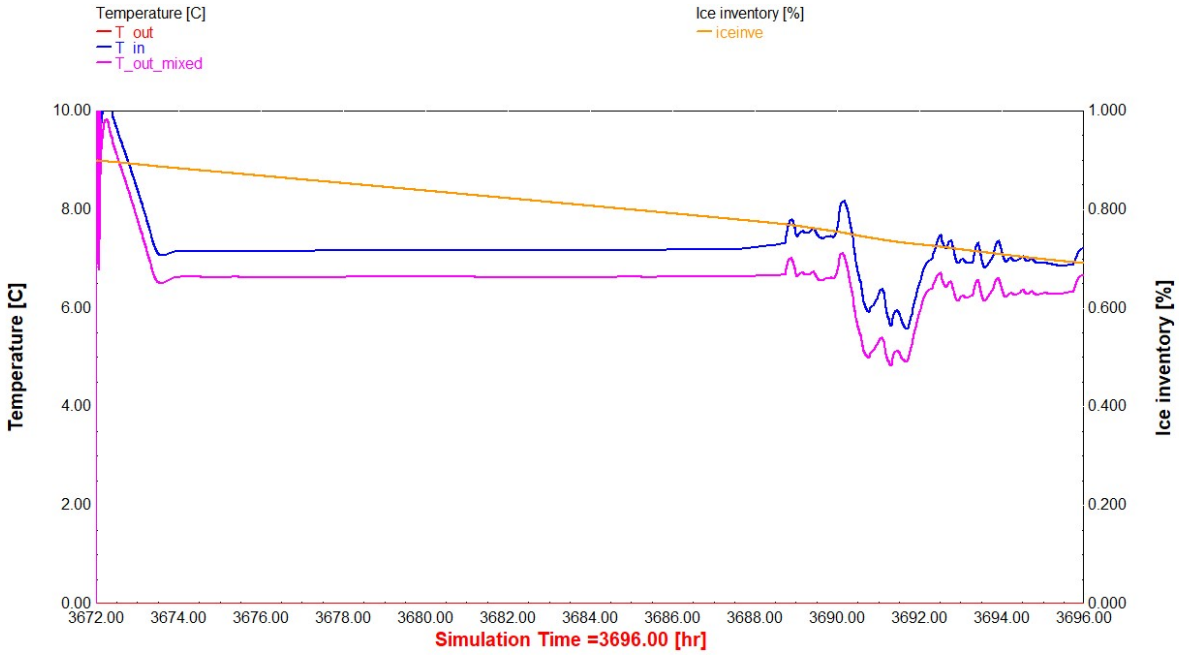

Figure 5.2: On the right axis, the temperatures of the tank's inlet T_{in} and outlet T_{out} are shown, as well as the leaving temperature after mixing $T_{out,mixed}$ with the TES bypass. On the left axis, the state of charge of the tank ice_{inve} is plotted and can be seen decreasing as the TES is discharged

Figure 5.3 shows the heat transfer rates in various components in the IBAL. As shown, the TES heat transfer rate matches the absolute value of the AHU heat transfer rate on the waterside. One thing worth noting is that the occupant load added by the occupants does not exactly match the corresponding air handling unit experienced load. This is explained by the cooling coil supply air setpoint temperature in the AHU.

As of now, the AHU supply air setpoint temperature is a constant value of 12C. When there are no occupants in the zones the load decreases; this results in the zone temperatures dropping, which results in the dampers closing to their minimum position. Once the dampers reach that position, the reheating element in the VAV box is turned on to maintain the zone temperatures at their set points. When the return air (at the zone temperatures) gets sent back to AHU for conditioning, the air temperature is higher than the 12C setpoint, thus, resulting in an experienced load across the cooling coils.

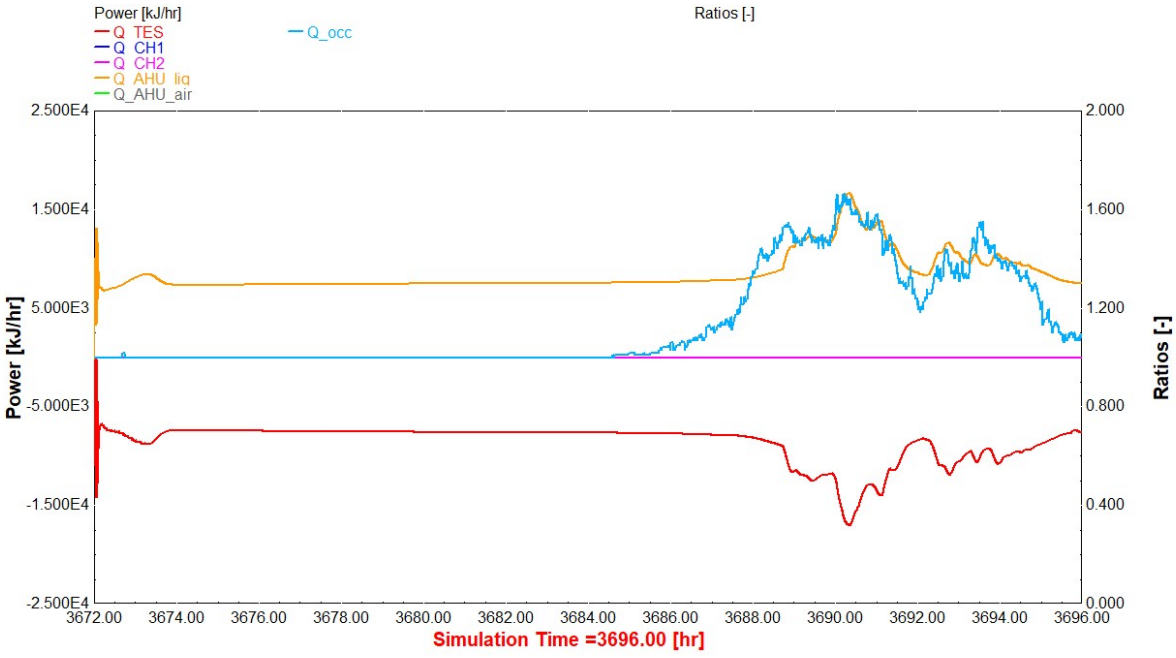

Figure 5.3: The heat transfer rates are plotted for different components in the IBAL. Since the TES is used to fully meet the demand, it can be seen that the TES heat transfer rate Q_{TES} is equivalent in absolute value to that of the air handling unit $Q_{AHU,liq}$.

Figure 5.4 and Figure 5.5 are used to demonstrate the response of the VAV box and

the cooling coil valves, respectively. The VAV box controller reacts to maintain the zone's setpoint temperatures. The control is accomplished by an algorithm that actuates the reheating element once the dampers are at their minimum positions, which was developed in [7].

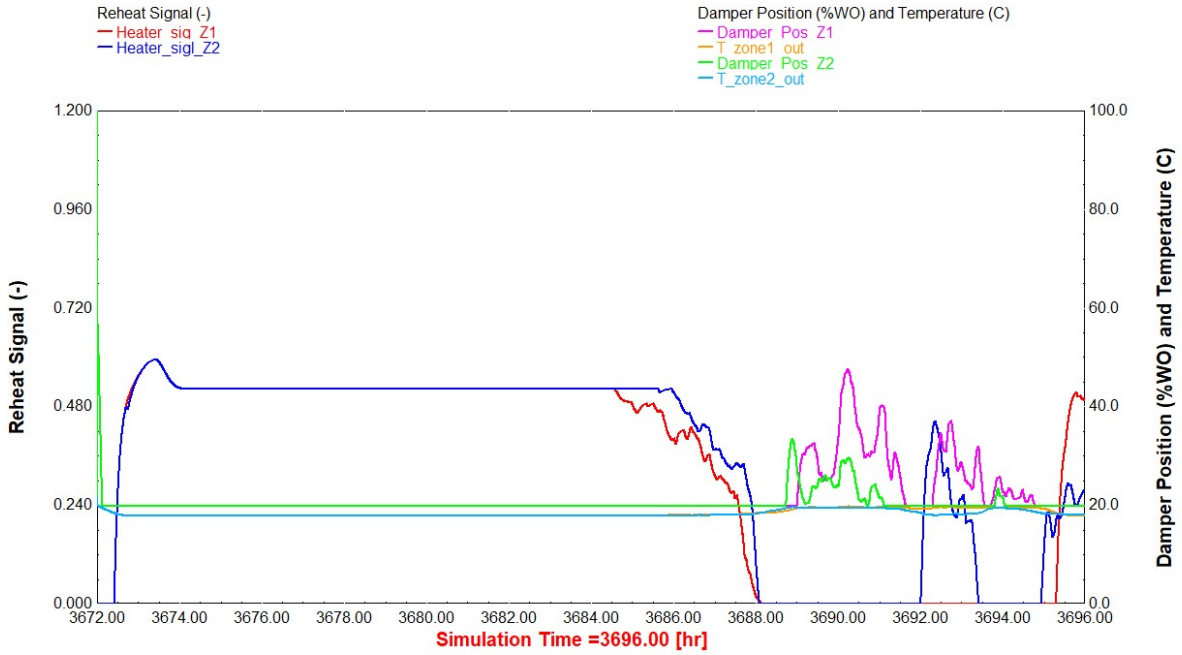

Figure 5.4: On the left axis, the preheating signals ($HeaterSig_{Z1}$ and $HeaterSig_{Z2}$) are plotted as it shows the varying intensity of the VAV heaters. On the right axis, the VAV damper positions ($DamperPos_{Z1}$ and $DamperPos_{Z2}$) and the zone temperatures are both plotted on the same axis.

The cooling coil controller modulates the chilled water flow rate to maintain a supply air setpoint temperature on the air-side system. Figure 5.5 shows the PID controller response to maintain the supply air temperature at a setpoint of 12C.

Primary Mode 3: Meet a cooling load using a chiller

In this mode, the chiller is solely used to meet the same building load in the previous case. Figure 5.6 illustrates the same outdoor weather conditions, zone sensible loads, as well as the regulated zone temperatures indicating proper temperature control.

Different from the previous case, the chiller power consumption is illustrated in Figure

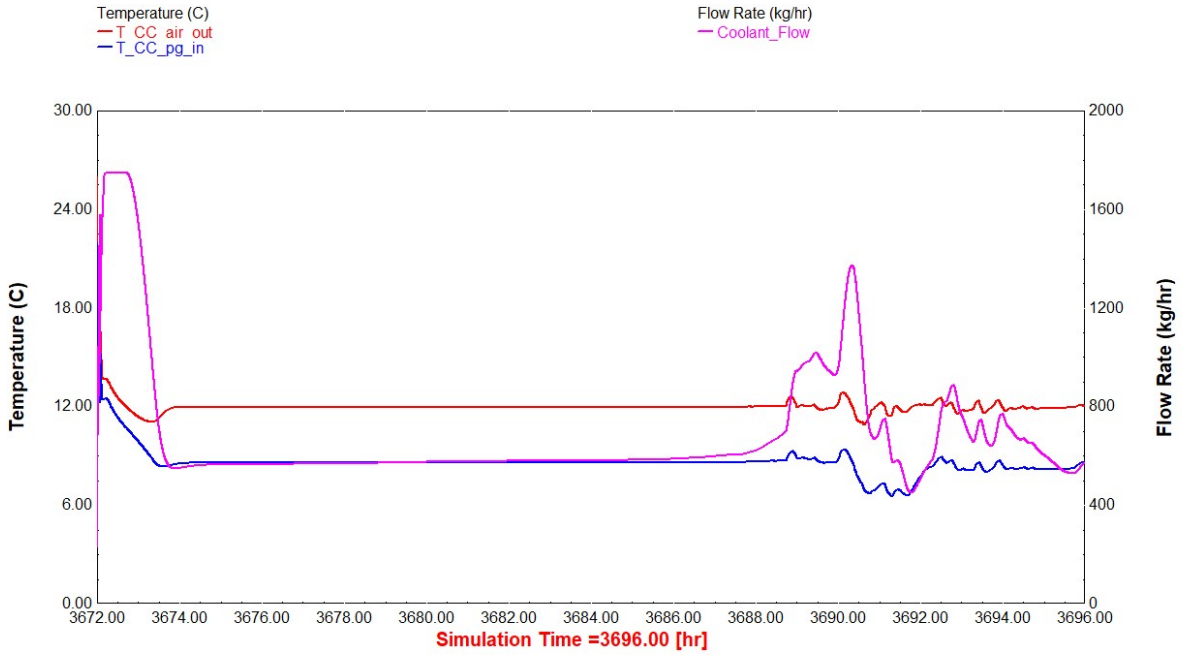

Figure 5.5: On the left axis, the temperatures of the air leaving $T_{cc,air,out}$ and the chilled water entering $T_{CC,pg,in}$ are shown. On the right axis, the chilled water flow rate $CoolantFlow$ is shown to demonstrate how it is modulated to maintain the supply air setpoint temperature.

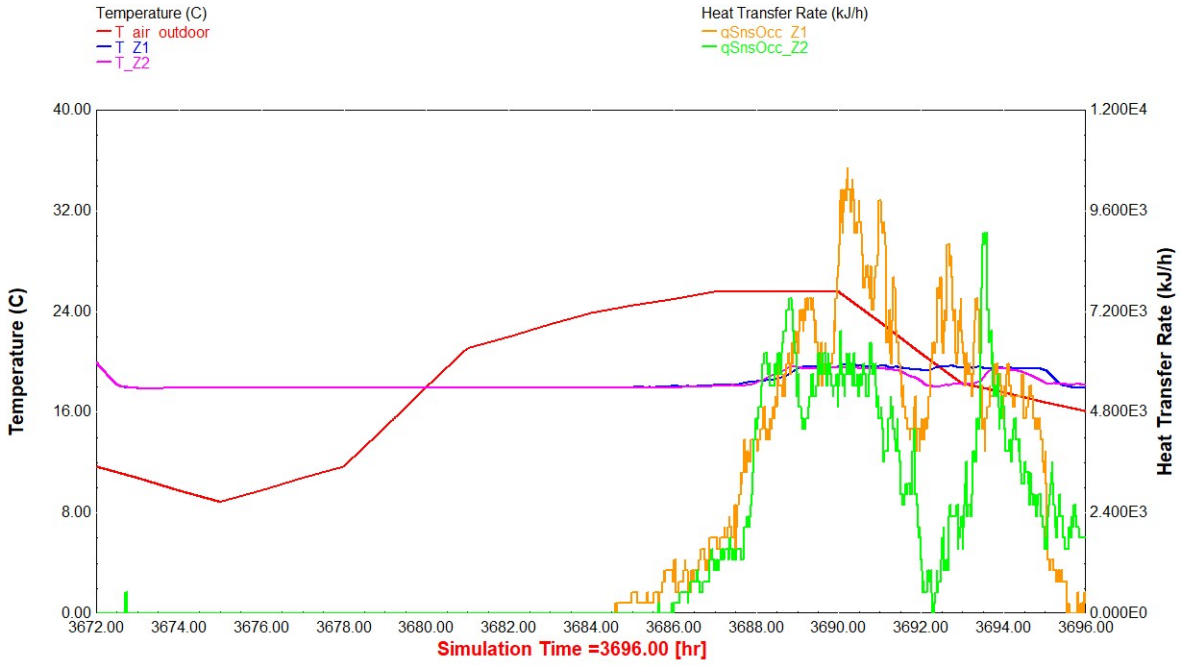

Figure 5.6: On the left axis, the outdoor air temperature $T_{air,outdoor}$ and the respective zone temperatures T_{Z1} and T_{Z2} are plotted. The zones are maintained at a setpoint temperature of 19C. On the right axis, the zones' sensible loads ($qSnsOcc_{Z1}$ and $qSnsOcc_{Z2}$) are plotted indicating the presence of occupants in the zones

5.7 instead to show the response of the chiller to the building demand. The chilled water temperature, the chilled water temperature setpoint, and the primary loop setpoint temperature are all shown. In this case, all the aforementioned temperatures overlap because Chiller 2 is used to meet the demand and the TES is not in operation.

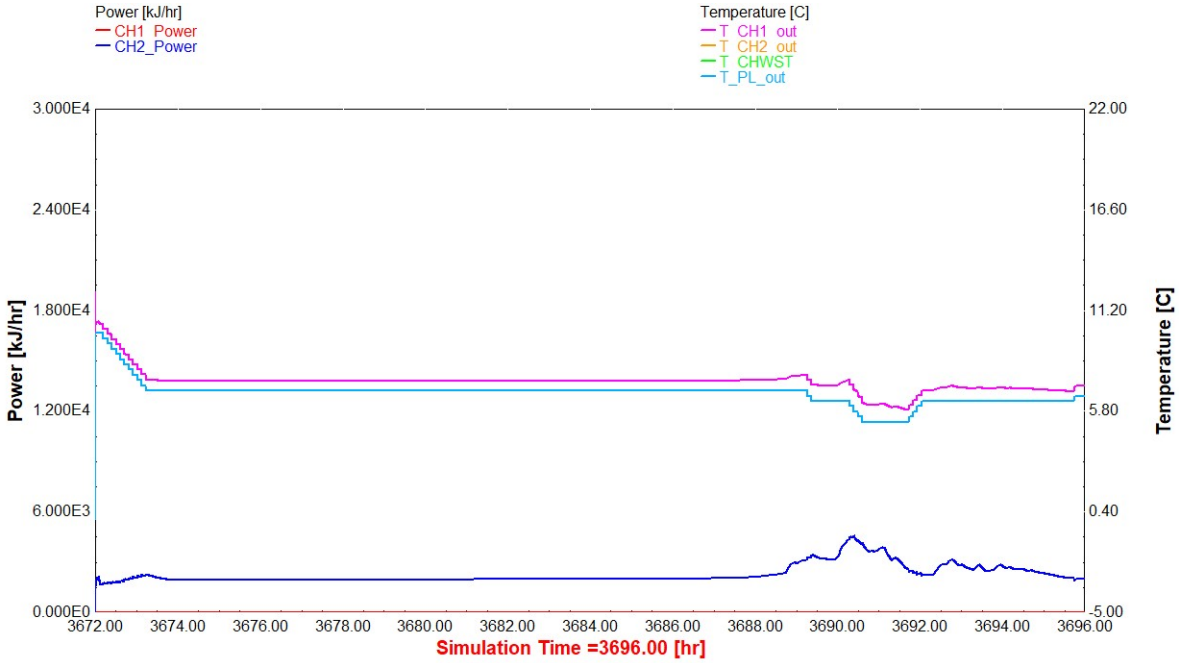

Figure 5.7: On the left axis, Chiller 2 power consumption $CH2_{Power}$ is plotted. On the right axis, the simulated chilled water temperature $T_{CH2,out}$, along with the set points for both the chilled water T_{CHWST} and primary loop temperatures $T_{PL,out}$

Figure 5.8 shows the loads in different components as presented in the previous case. As seen, the load met by chiller 2 matches that of the air handling unit with a slight offset. The offset can be explained by the fact that the chilled water flow rate in the primary loop is greater than that of the secondary loop, which leads to the chilled water supply blending with the secondary loop returning water and reducing its temperature. As a result, the water entering the chillers is slightly colder than that leaving the AHU.

As with the previous case, Figure 5.9 and Figure 5.10 are used to demonstrate the response of the VAV box and the cooling coil valve, respectively. The VAV box controllers react to maintain the same zone's setpoint temperatures, and the cooling coil controller

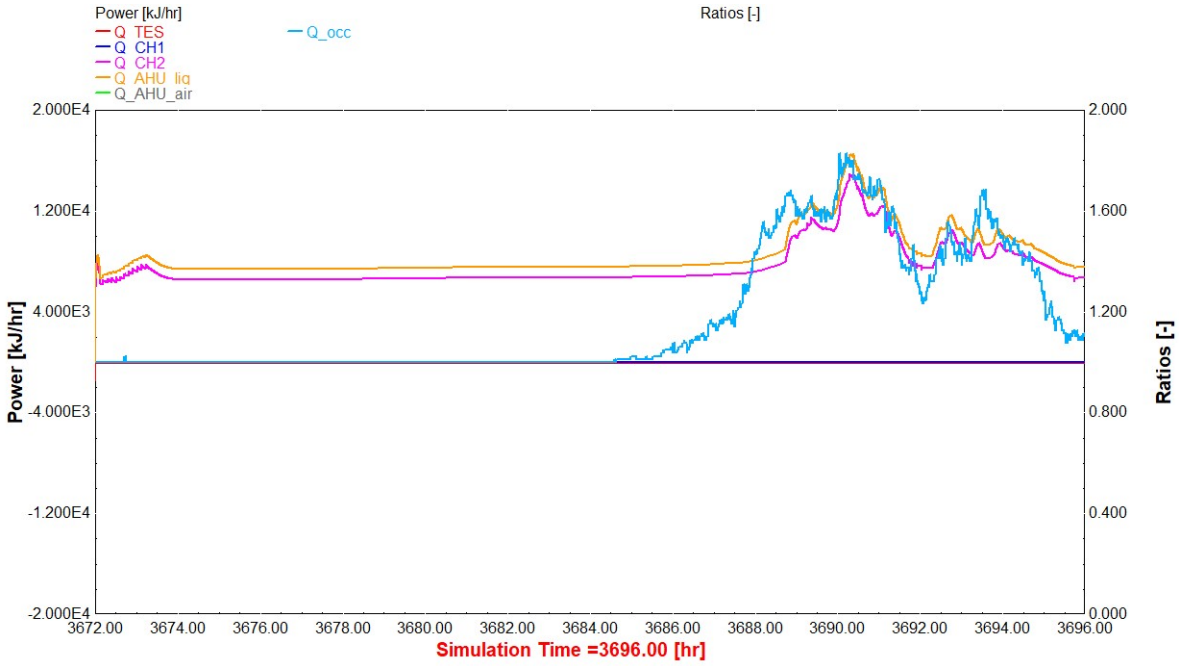

Figure 5.8: The heat transfer rates are plotted for different components in the IBAL. Since chiller 2 is used to fully meet the demand, it can be seen that the respective heat transfer rate Q_{CH2} is equivalent in absolute value to that of the air handling unit $Q_{AHU,liq}$.

modulates the chilled water flow rate to maintain the same supply air setpoint temperature on the air-side system.

Primary Mode 5: Charge the TES with ice and meet a load in the secondary loop

This case demonstrates the TES charging fully from an initial SOC of 10% while meeting the zone occupant loads at the same time. As with the previous case, Figure 5.11 illustrates the same outdoor condition and occupant loads, as well as the zones' regulated temperatures that indicate proper control relative to the setpoint of 19C.

Since the TES is charged by building ice, Figure 5.12 illustrates that process as time progresses. It should be noted that the discontinuity that occurs in the outlet temperature once the TES is fully charged is not exactly physical. In a real system, the TES will first undergo sensible charging until the phase change material (in this case, water) reaches its freezing temperature, after which latent charging occurs and ice forms during this

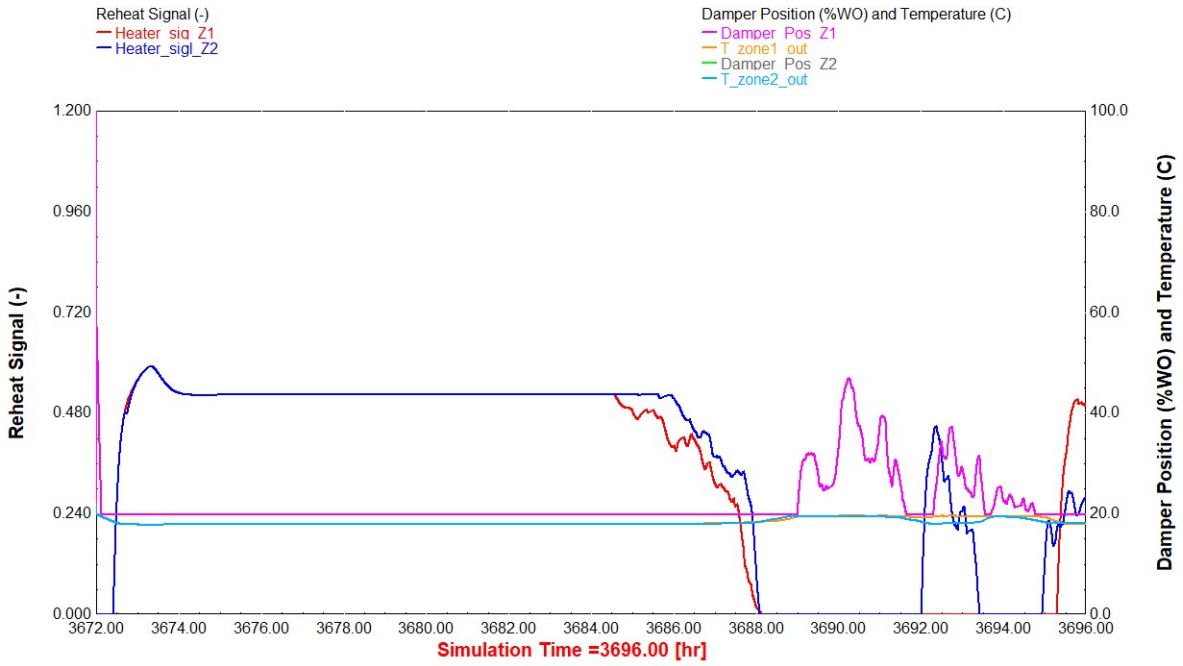

Figure 5.9: On the left axis, the preheating signals ($\mathtt{HeaterSig}_{Z1}$ and $\mathtt{HeaterSig}_{Z2}$) are plotted as it shows the varying intensity of the VAV heaters. On the right axis, the VAV damper positions ($\mathtt{DamperPos}_{Z1}$ and $\mathtt{DamperPos}_{Z2}$) and the zone temperatures are both plotted on the same axis.

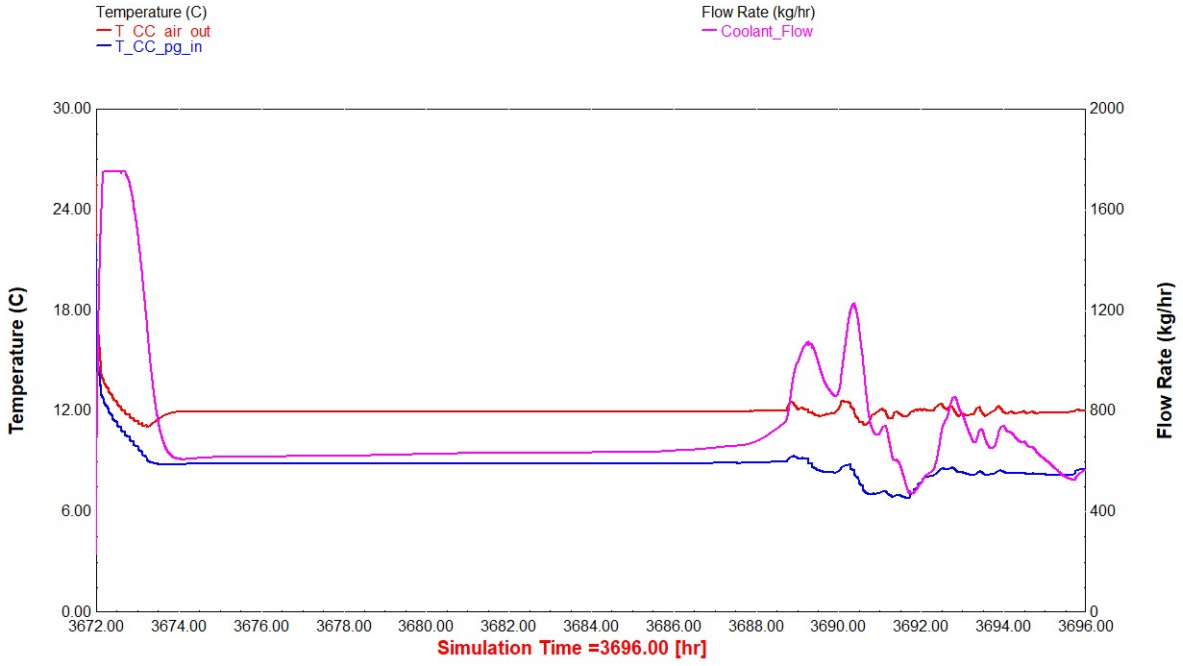

Figure 5.10: On the left axis, the temperatures of the air leaving $\mathrm{T}_{\mathtt{cc,air,out}}$ and the chilled water entering $\mathrm{T}_{\mathtt{CC,pg,in}}$ are shown. On the right axis, the chilled water flow rate $\mathtt{CoolantFlow}$ is shown to demonstrate how it is modulated to maintain the supply air setpoint temperature.

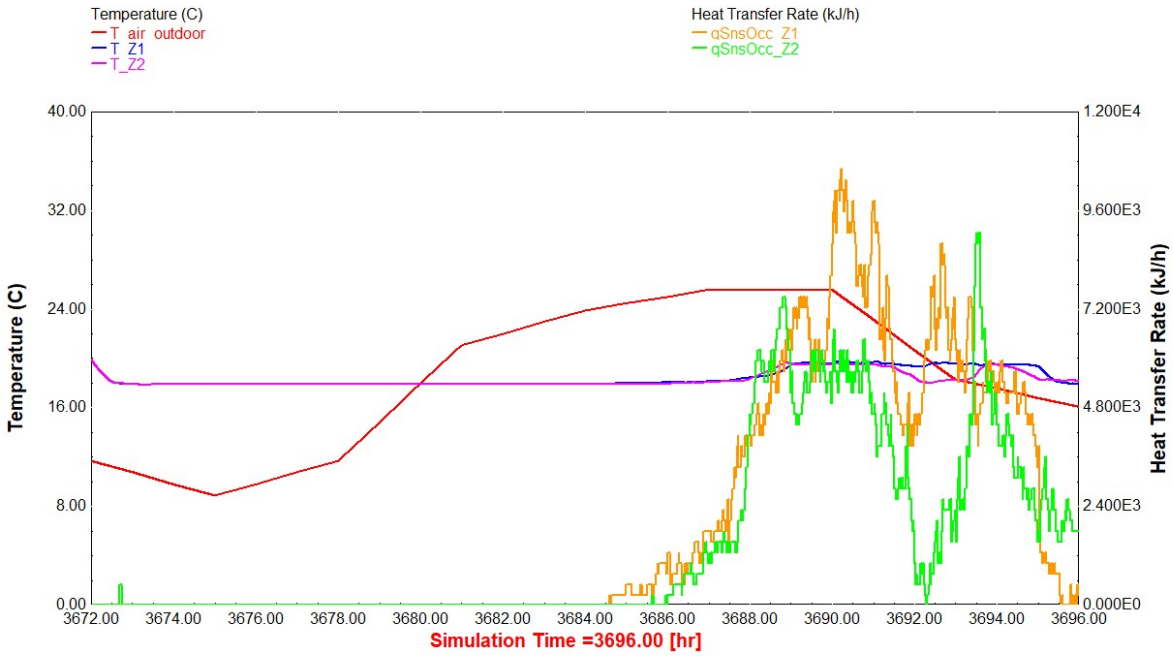

Figure 5.11: On the left axis, the outdoor air temperature $T_{air,outdoor}$ and the respective zone temperatures T_{Z1} and T_{Z2} are plotted. The zones are maintained at a setpoint temperature of 19C. On the right axis, the zones' sensible loads ($qSnsOcc_{Z1}$ and $qSnsOcc_{Z2}$) are plotted indicating the presence of occupants in the zones

stage. In the real world, this behavior would result in the leaving heat transfer fluid (30% PG water mixture) temperature to approach zero temperature difference relative to the ice temperature.

The chiller power consumption is illustrated in Figure 5.13 to show the response of the chiller to charging the TES. The chilled water temperature, the chilled water temperature setpoint, and the primary loop setpoint temperature are also shown. In this case, the chilled water setpoint temperature is set at an ice-making temperature, while the primary loop outlet setpoint temperature is set such that it meets the demand load in the secondary loop imposed by the occupant loads.

The temperatures at the inlets and outlets of the primary and secondary loops are shown in Figure 5.14. Given that the TES is being charged, the TES valve is fully open and the temperature leaving the primary loop is at an ice-making temperature. However,

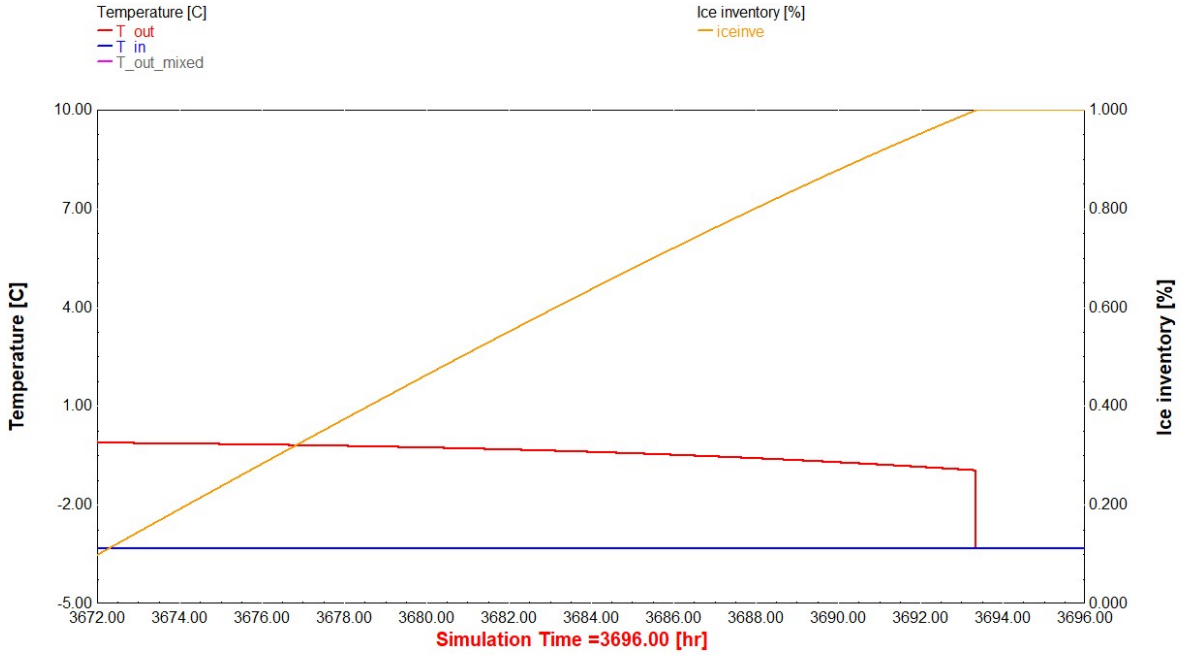

Figure 5.12: On the left axis, the temperature of the entering T_{in} and leaving T_{out} chilled water is plotted. Since the TES is being charged, the TES valve is fully open and all the flow goes through the TES; this is why the final mixed leaving temperature $T_{out,mixed}$ is omitted since there is no mixing. On the right axis, the TES state of charge ice_{inve} is plotted to demonstrate the charging process.

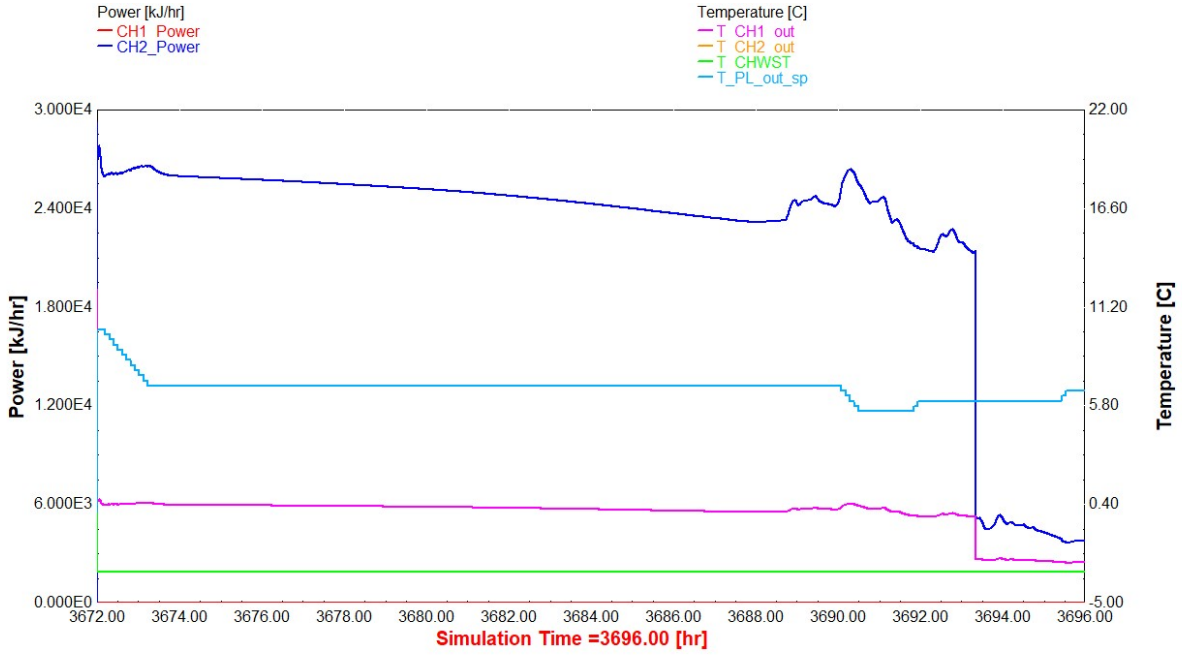

Figure 5.13: On the right axis, the power of chiller 2 $CH2_{Power}$ is plotted to demonstrate the charging process. On the right axis, the chilled water temperature $T_{CH2,out}$, and the set points for both the chilled water T_{CHWST} and primary loop outlet $T_{PL,out}$ temperatures

the bridge valve is used to bypass the primary flow to achieve the secondary loop inlet temperature. The bypass effect can also be inferred from the difference between the temperature leaving the secondary loop $T_{SL,out}$ and the temperature entering the primary loop $T_{PL,in}$. In this case, most of the water leaving the ice tank is bypassed to the primary loop inlet leading to the temperature difference seen.

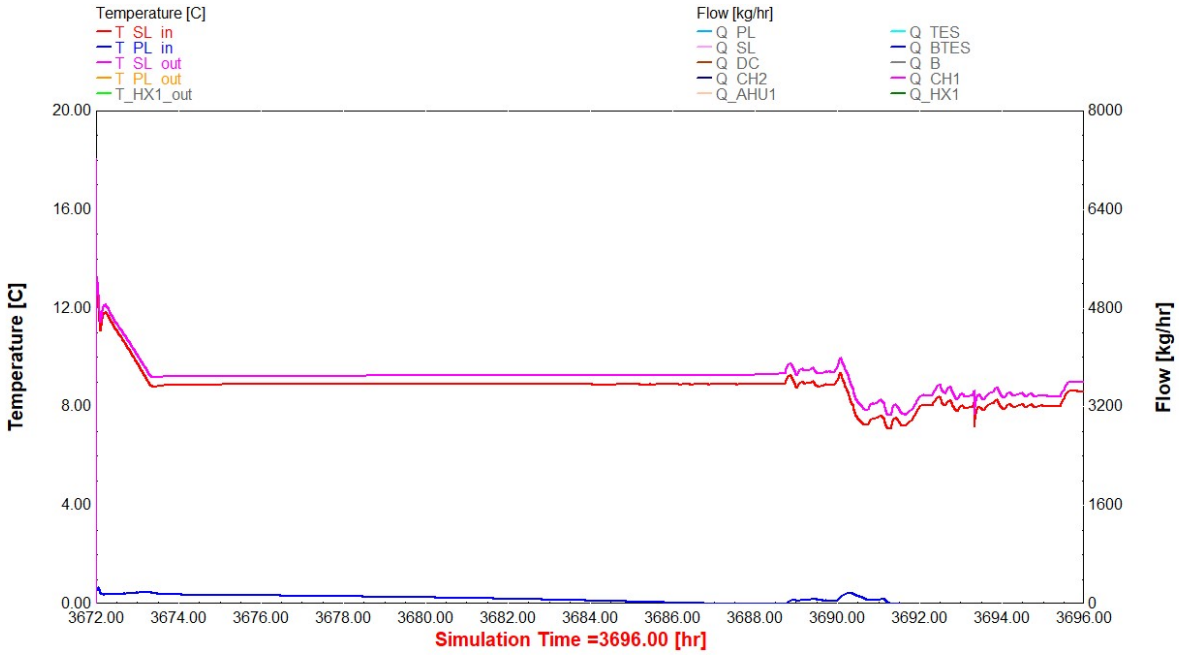

Figure 5.14: The inlet and outlet temperatures of the primary loop $T_{PL,in}$ and $T_{PL,in}$, respectively, as well as the inlet and outlet temperatures of the secondary loops $T_{SL,in}$ and $T_{SL,in}$, respectively.

Figure 5.15 is used to demonstrate the cooling coil valve controller. Similar to before, this controller modulates the chilled water flow rate in the hydronic system to maintain a supply air setpoint temperature in the air-side system, which is accomplished even during TES charging.

Case 2: Multi-mode simulation

To showcase an example of multiple modes executed in the same simulation, a mode schedule is generated using the MPC discussed in Chapter 4. The MPC is provided with a utility time-of-use rate structure, along with the same building occupant demand profile

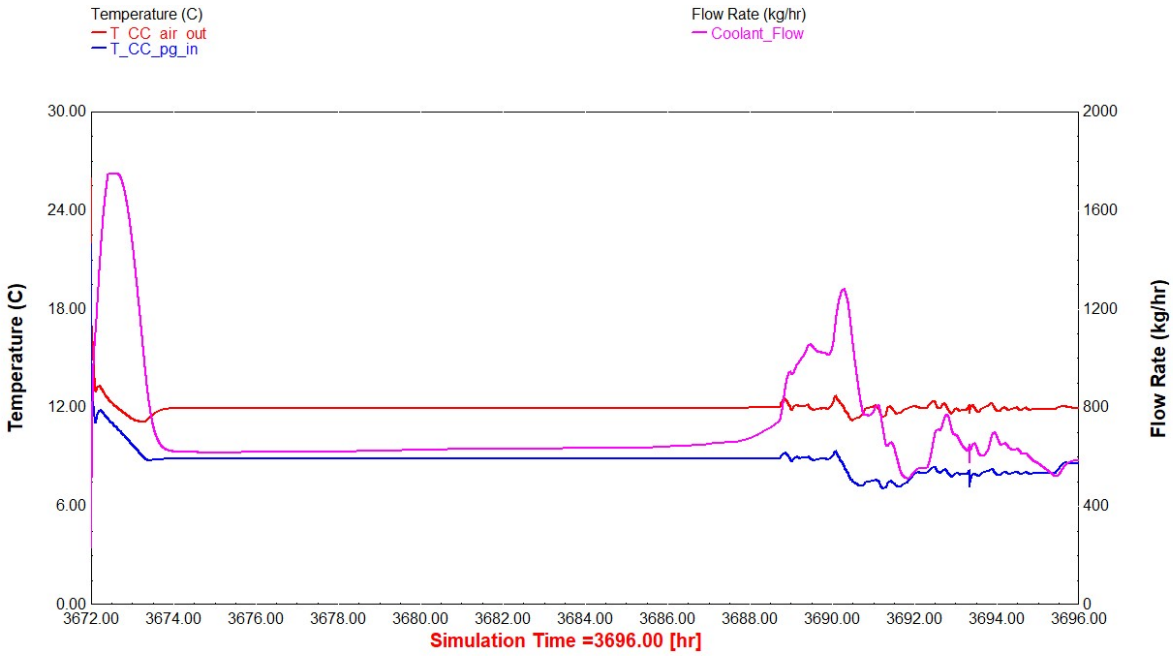

Figure 5.15: On the left axis, the temperature of the air leaving $T_{cc,air,out}$ and the chilled water entering $T_{CC,pg,in}$ is shown. On the right axis, the chilled water flow rate $CoolantFlow$ is shown to demonstrate how it is modulated to maintain the supply air setpoint temperature while the chiller is charging the TES.

scaled to double, as inputs. The load scaling is performed to place a higher load on the IBAL relative to it's cooling capacity. Figure 5.16 illustrates the schedule of the electricity price from the Wisconsin Public Service three-tier time-of-use program [15], where the electricity price changes based on the time of the day. Meanwhile, Figure 5.17 shows the occupant load that the chiller and TES need to meet.

The MPC is developed in a Python script that uses the Gurobi optimization engine as the optimization solver. The script is executed to generate a schedule of the optimal, cost-minimizing sequence of the IBAL operation modes. In this case, the MPC is formulated such that it is limited to choosing between three modes: charge the TES with ice, meet demand with the TES, or meet demand with the chiller. The schedule of the primary modes is exported from the Python script to a text file, which also includes the secondary mode set to 2 (i.e. use chiller 2 and/or its respective pump/flow branch).

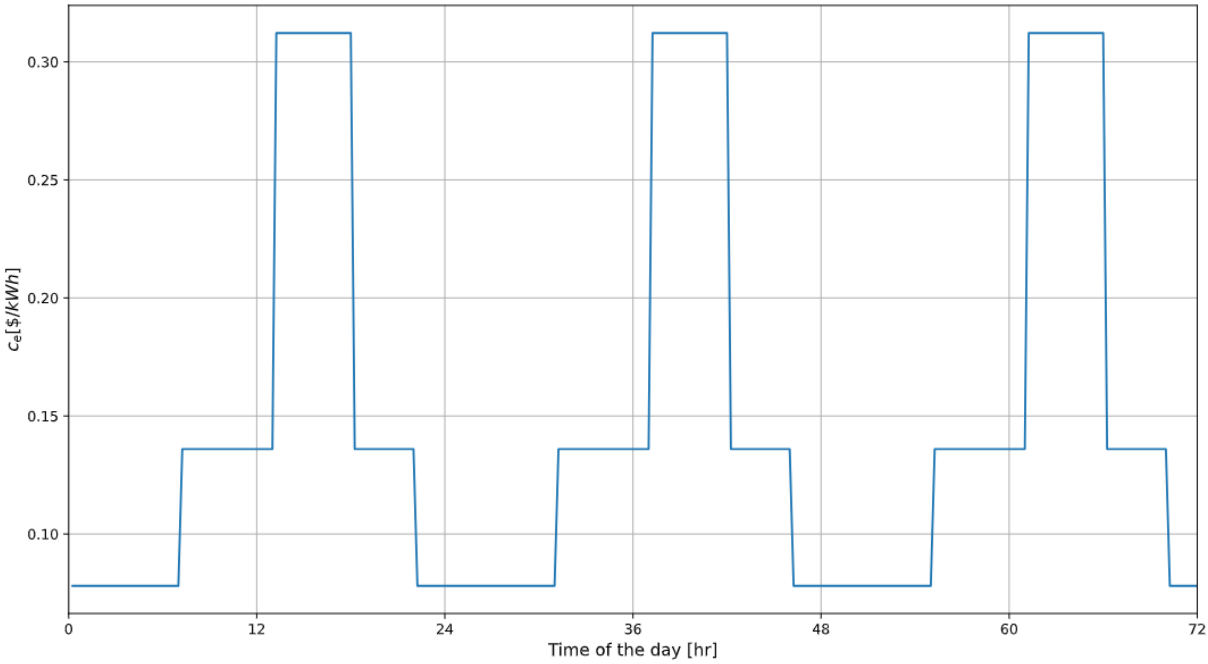

Figure 5.16: Electricity price schedule based on a Time-of-Use structure.

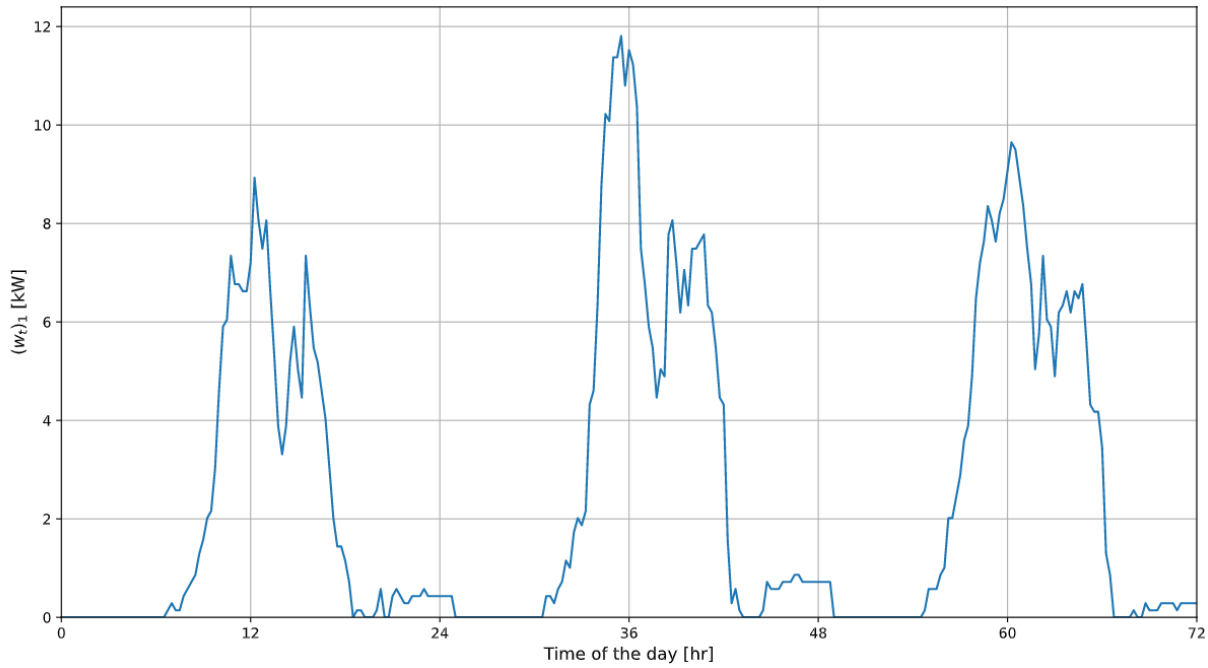

Figure 5.17: Occupant thermal load from the zones represents the "building" load in the IBAL that the hydronic system responds to.

Figure 5.18 shows the schedule of the MPC-generated modes. One modification performed to the MPC schedule is converting the charge TES mode (mode 2 in the TRNSYS model) to charge TES and meet demand (mode 5 in the TRNSYS model). This is done to address the constant thermal load applied by the VAV even when no occupant thermal load is present, which was discussed in more detail in the previous chapter.

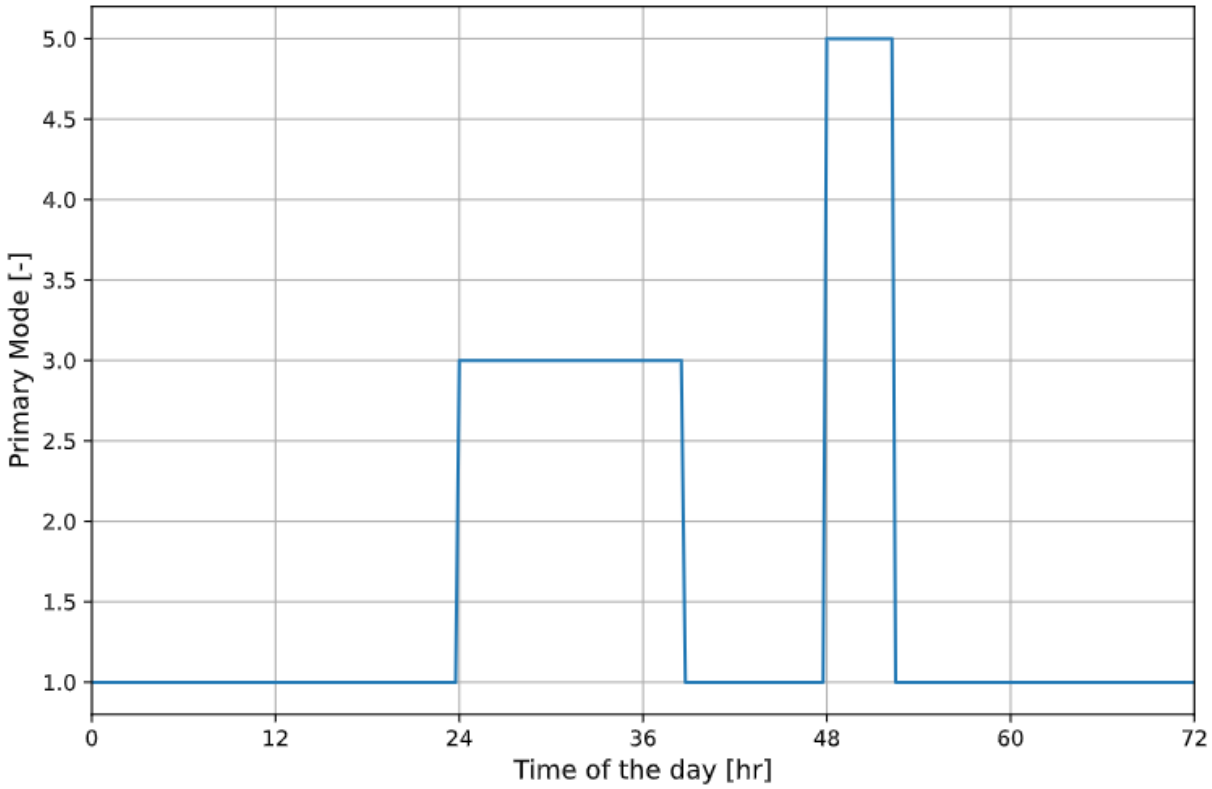

Figure 5.18: The MPC-generated primary mode schedule of the IBAL over an optimization period of 72 hours. Mode 1 uses TES to meet demand, mode 3 uses the chiller to meet demand, and mode 5 charges the TES with ice.

Once the mode schedule is provided to TRNSYS, a simulation that spans the three-day period of the IBAL is executed. Figure 5.19 and Figure 5.20 compare the TRNSYS TES state of charge prediction to its equivalent from the MPC, respectively. As shown, the TRNSYS simulation diverges from the MPC prediction during instances when there is no occupant thermal load, but the VAV boxes add thermal load. The result of that is discharging the TES in TRNSYS more than predicted by the MPC.

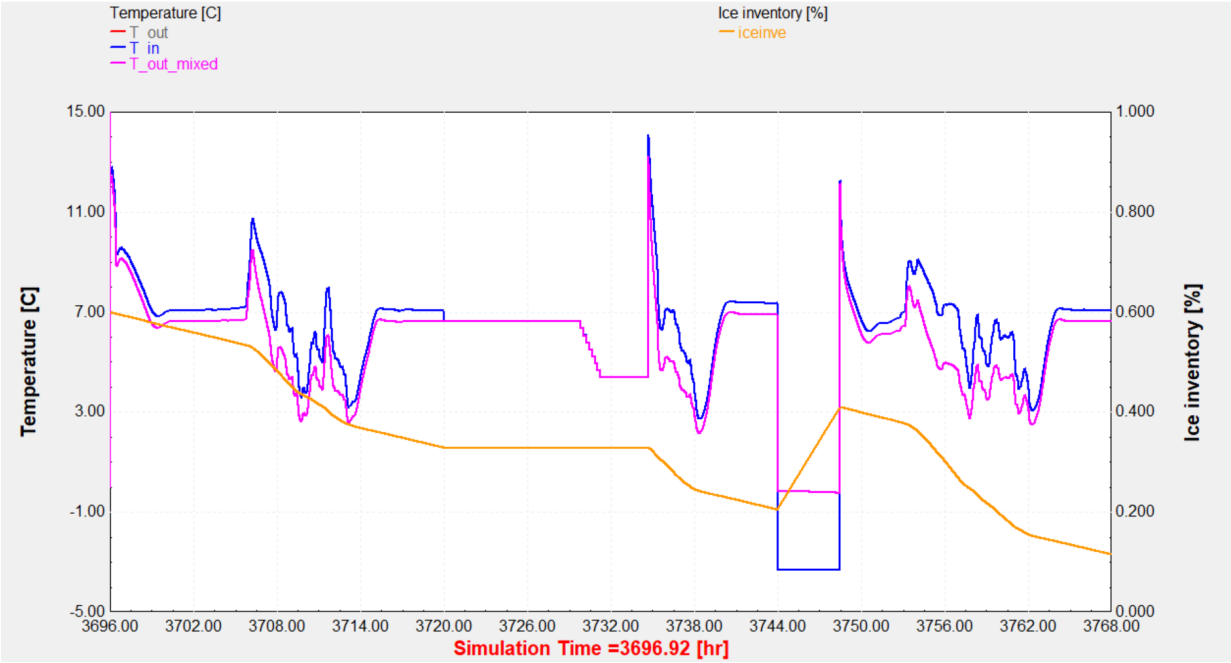

Figure 5.19: The state of the TES from the TRNSYS simulation using the MPC mode schedule. On the left axis, the TES inlet temperature T_{in}, and mixed outlet temperature $T_{out,mixed}$ are shown. On the right axis, the TES state of charge is plotted.

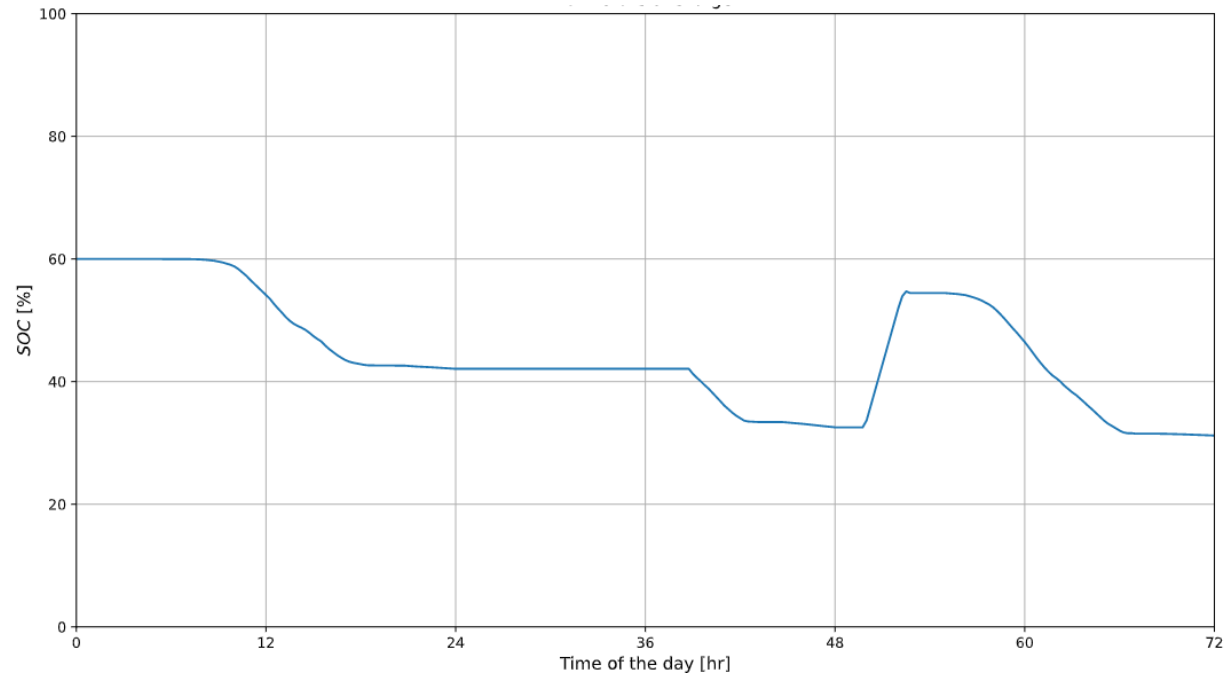

Figure 5.20: The predicted state of charge of the TES from the MPC solution.

Figure 5.21 illustrates the response of the VAV boxes to maintain the zone temperature setpoints of 19C. During periods when there are no occupants, the dampers close to their minimum position and the reheating elements are activated. As a result, a thermal load is experienced by the hydronic system during those periods of time, which is shown in Figure 5.22

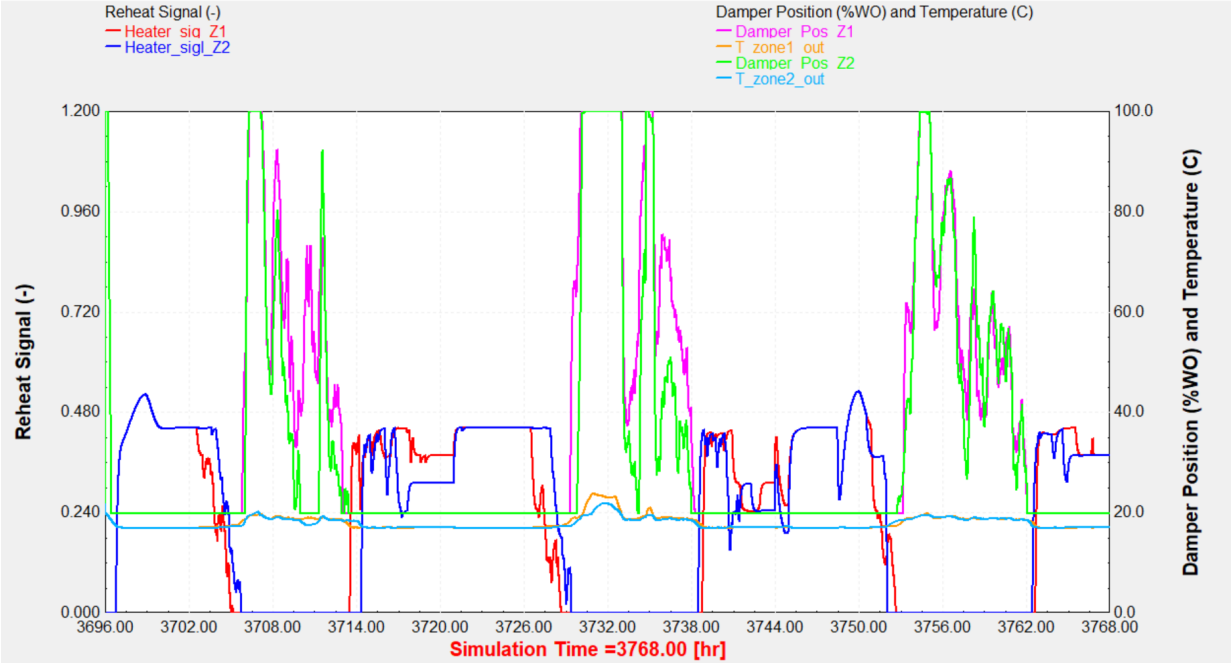

Figure 5.21: The VAV boxes respond to maintain the zone temperature during the MPC-generated schedule TRNSYS simulation. On the left axis, the preheating signals ($HeaterSig_{Z1}$ and $HeaterSig_{Z2}$) are plotted as it shows the varying intensity of the VAV heaters. On the right axis, the VAV damper positions ($DamperPos_{Z1}$ and $DamperPos_{Z2}$) and the zone temperatures are both plotted on the same axis.

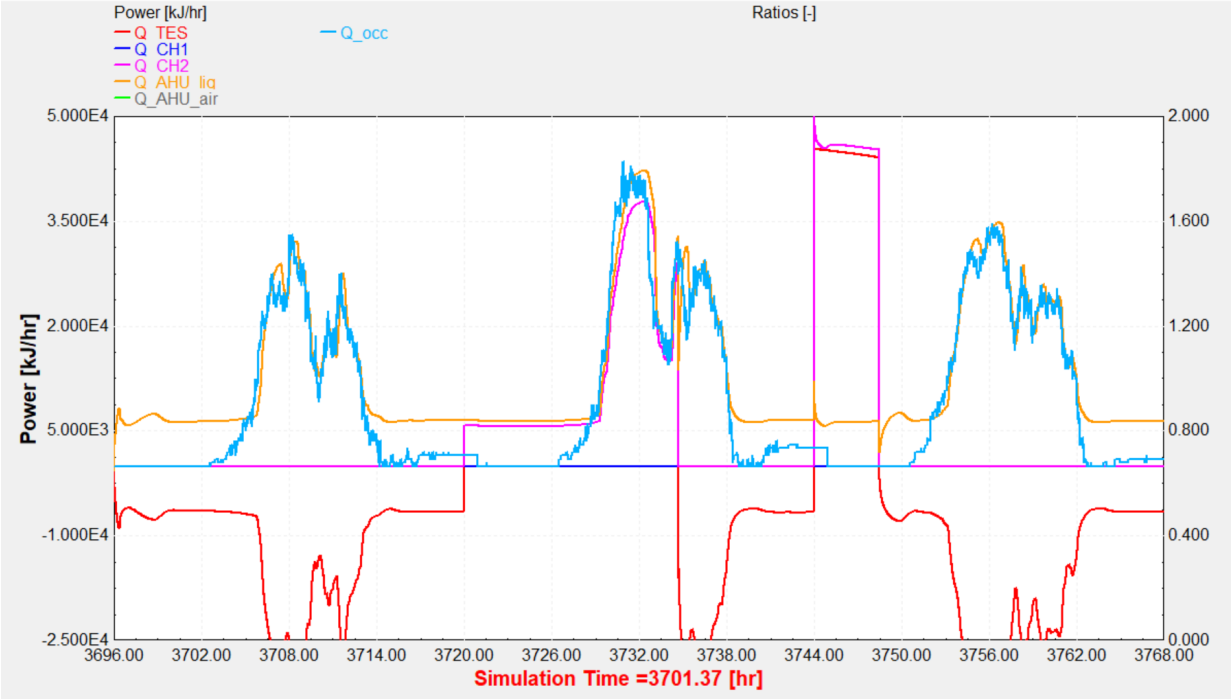

Figure 5.22: The heat transfer rates are plotted for different components in the IBAL during a simulation that uses an MPC-generated mode schedule.

6 CONCLUSIONS

This project embarks on creating a comprehensive TRNSYS model capable of simulating the IBAL's performance. In order to achieve that, first, the IBAL's hydronic system components are characterized and modeled using either standard TRNSYS models or custom-made models. Second, the hydronic system model is integrated with the previously developed air-side system model. Third, operation modes are defined for the complete IBAL TRNSYS model and demonstrated using a test case with sample weather and occupancy data. Lastly, a TES dispatch model predictive controller is developed to demonstrate the promise of that control strategy in optimizing HVAC operation.

As a result of capturing the hydronic system's performance, it is made possible to model the different components such as the chillers, pumps, and TES at the appropriate level of fidelity in TRNSYS. By integrating these developed models with the air-side system, the outcome of that is a TRNSYS model that serves as a tool for researchers alike. This tool can be used for applications ranging from energy usage case studies to an online digital twin run in conjunction with an intelligent controller, which an example of is demonstrated with the developed TES dispatch MPC.

Overall, this project carries great potential for adding a meaningful contribution to the building energy research field, and more broadly to renewable energy research. Many aspects of this project can be further explored and analyzed to obtain greater insight into potential intelligent energy optimization solutions.

7 FUTURE WORK

As the TRNSYS model is used more by researchers to conduct different types of experimentation, it could be possible that some models may require a higher level of physical detail. The TES is an example of a model that is currently a simple Effectiveness-NTU-based model. An upgrade for this model can take the form of a detailed model that captures the different physical phenomenons of the phase change material. An example of such a model was developed by [16].

A related outcome to the previous limitation is that the effects of partial charging and discharging events are not accounted for in this model. In a situation where a discharge event occurs after a partial charge, the formation of a water annulus around the tubes traps a layer of ice, effectively reducing the tank's storage capacity. Equivalently, during a charging event that follows a partial discharge, once the ice forming around the tubes intersects with the trapped layer of ice, the heat transfer resistance experiences a discontinuity. Incorporating a more detailed TES model will also overcome the issue of what happens beyond a SOC of 100% or less than 0%. A more physical model would account for the thermal capacitance of the tank, as well as the temperature change of the phase change material, throughout all the different TES phases.

Nevertheless, since the model's purpose is to aid the development of primarily intelligent control methods, the time scale that these controllers often deal with is the span of minutes to hours (and sometimes days). This provides leeway for having low-fidelity models that mainly capture the high-level steady-state behavior, and are less concerned about low-level transient behavior. A downside of that would be a decreased accuracy for relatively long simulations when the effect of these simplifications starts to appear, which could make it necessary to limit the length of the simulated time.

An example of how this model can be utilized as a tool is in an online control loop. For instance, a supervisory intelligent agent can obtain the initial state of the physical IBAL, generate an operation schedule for a control horizon, execute that control horizon schedule in TRNSYS, update the intelligent agent with the TRNSYS predicted system state, and optimize the next control horizons, and update the intelligent agent using the physical IBAL's states after a given time/horizons.

Lastly, an overall validation would be valuable to ensure that the TRNSYS model matches the physical IBAL on a system level. The components were developed using data collected on a component level, where each component is "isolated" in the test runs. Running test cases in the real IBAL and comparing them to the TRNSYS model can be an appropriate way to stress-test the model, as well as tune the model to increase the accuracy even further.

REFERENCES

[1] Schwenzer, Max, Muzaffer Ay, Thomas Bergs, and Dirk Abel. 2021. Review on model predictive control: an engineering perspective. *The International Journal of Advanced Manufacturing Technology* 117:1–23.

[2] Kopach, Adam J. 2021. Modeling of the nist intelligent building agents laboratory. Master's thesis, University of Wisconsin-Madison.

[3] U.S. Energy Information Administration. 2018. Energy use in commercial buildings. `https://www.eia.gov/energyexplained/use-of-energy/commercial-buildings-in-depth.php` [Accessed: 2023-08-24].

[4] Kelly, Steven, George & Bushby. 2012. Are intelligent agents the key to optimizing building hvac system performance? *Hvac & Research* 18:750–759.

[5] Pertzborn, A. J. 2016. Intelligent building agents laboratory: Hydronic system design (nist technical note 1933).

[6] Pertzborn, A. J & Veronica D. A. 2018. Intelligent building agents laboratory: air system design (nist technical note 2025).

[7] ———. 2021. Baseline control systems in the intelligent building agents laboratory (nist technical note 2178).

[8] Solar Energy Lab. 2023. Trnsys 18. `https://sel.me.wisc.edu/trnsys/features/features.html` [Accessed: 2023-08-24].

[9] Afroz, Zakia, GM Shafiullah, Tania Urmee, and Gary Higgins. 2018. Modeling techniques used in building hvac control systems: A review. *Renewable and Sustainable Energy Reviews* 83:64–84.

[10] Nellis, S. Klein & G. 2011. *Thermodynamics*. Cambridge University Press.

[11] Tang, Rui, and Shengwei Wang. 2019. Model predictive control for thermal energy storage and thermal comfort optimization of building demand response in smart grids. *Applied Energy* 242:873–882.

[12] Ma, Yudong, Francesco Borrelli, Brandon Hencey, Andrew Packard, and Scott Bortoff. 2009. Model predictive control of thermal energy storage in building cooling systems. In *Proceedings of the 48h ieee conference on decision and control (cdc) held jointly with 2009 28th chinese control conference*, 392–397.

[13] Kircher, K. Max, Kevin J. & Zhang. 2015. Model predictive control of thermal storage for demand response. In *2015 american control conference (acc)*, 956–961.

[14] Luo, Na, Zhe Wang, David Blum, Christopher Weyandt, Norman Bourassa, Mary Ann Piette, and Tianzhen Hong. 2022. A three-year dataset supporting research on building energy management and occupancy analytics. *Scientific Data* 9(1).

[15] Service, Wisconsin Public. 2023. Three-tier time-of-use.

[16] Jekel, Todd B. 1991. Modeling of ice-storage systems. Master's thesis, University of Wisconsin-Madison.